SPECIAL REPORT RDMR-AD-16-03

TEST DATA REPORT, LOW-SPEED WIND TUNNEL DRAG TEST OF A 2/5 SCALE LOCKHEED AH-56 CHEYENNE DOOR-HINGE HUB

Robert D. Vocke III and Gerardo Nuñez
Aviation Development Directorate
Aviation and Missile Research, Development, and Engineering Center

July 2016

Distribution Statement A: Approved for public release; distributed is unlimited.

DESTRUCTION NOTICE

DISCLAIMER

TRADE NAMES

REPORT DOCUMENTATION PAGE			Form Approved OMB No. 074-0188
Public reporting burden for this collection of information is estimated to average 1 hour per response, including the time for reviewing instructions, searching existing data sources, gathering and maintaining the data needed, and completing and reviewing this collection of information. Send comments regarding this burden estimate or any other aspect of this collection of information, including suggestions for reducing this burden to Washington Headquarters Services, Directorate for Information Operations and Reports, 1215 Jefferson Davis Highway, Suite 1204, Arlington, VA 22202-4302, and to the Office of Management and Budget, Paperwork Reduction Project (0704-0188), Washington, DC 20503			
1. AGENCY USE ONLY	2. REPORT DATE July 2016	3. REPORT TYPE AND DATES COVERED Final	
4. TITLE AND SUBTITLE Test Data Report, Low-Speed Wind Tunnel Drag Test of a 2/5 Scale Lockheed AH-56 Cheyenne Door-Hinge Hub			5. FUNDING NUMBERS
6. AUTHOR(S) Robert D. Vocke III and Gerardo Nuñez			
7. PERFORMING ORGANIZATION NAME(S) AND ADDRESS(ES) Commander, U.S. Army Research, Development, and Engineering Command ATTN: RDMR-ADF-TC Redstone Arsenal, AL 35898-5000			8. PERFORMING ORGANIZATION REPORT NUMBER SR-RDMR-AD-16-03
9. SPONSORING / MONITORING AGENCY NAME(S) AND ADDRESS(ES)			10. SPONSORING / MONITORING AGENCY REPORT NUMBER
11. SUPPLEMENTARY NOTES			
12a. DISTRIBUTION / AVAILABILITY STATEMENT Approved for public release; distribution is unlimited.			12b. DISTRIBUTION CODE A
13. ABSTRACT (Maximum 200 Words) The Aviation Development Directorate of the U.S. Army Aviation and Missile Research, Development and Engineering Center (AMRDEC) conducted a drag test of a non-rotating 2/5 scale Lockheed AH-56 Cheyenne main rotor hub in the U.S. Army 7– by 10–foot Wind Tunnel located at NASA Ames Research Center in Moffett Field, CA. The purpose of the test was to quantify the drag reduction on the Cheyenne's unique "door hinge" style hub when the mechanical control gyro is removed, with the implicit assumption that the control and stabilization functions of the gyro could be replaced by a modern flight control system located somewhere within the aircraft's outer mold line. The model was tested in a number of non-rotating configurations, orientations, and tunnel conditions. Baseline results compared favorably with historical drag measurements, and showed approximately a 50% reduction in hub drag with the gyro removed, with an additional 10% reduction due to rudimentary streamlining of the bluff outer hub arm.			
14. SUBJECT TERMS Hub Drag, Wind Tunnel, AH-56, Compound Helicopter			15. NUMBER OF PAGES
			16. PRICE CODE
17. SECURITY CLASSIFICATION OF REPORT UNCLASSIFIED	18. SECURITY CLASSIFICATION OF THIS PAGE UNCLASSIFIED	19. SECURITY CLASSIFICATION OF ABSTRACT UNCLASSIFIED	20. LIMITATION OF ABSTRACT SAR

NSN 7540-01-280-5500

Standard Form 298 (Rev. 2-89)
Prescribed by ANSI Std. Z39-18
298-102

Test Data Report, Low-Speed Wind Tunnel Drag Test of a 2/5 Scale Lockheed AH-56 Cheyenne Door-Hinge Hub

Robert D Vocke III   Gerardo Nuñez
Aviation Development Directorate
U.S. Army Aviation and Missile research, Development and Engineering Center

July, 2016

Summary

The Aviation Development Directorate of the U.S. Army Aviation and Missile Research, Development and Engineering Center (AMRDEC) conducted a drag test of a non-rotating 2/5 scale Lockheed AH-56 Cheyenne main rotor hub in the U.S. Army 7– by 10–foot Wind Tunnel located at NASA Ames Research Center in Moffett Field, CA. The purpose of the test was to quantify the drag reduction on the Cheyenne's unique "door hinge" style hub when the mechanical control gyro is removed, with the implicit assumption that the control and stabilization functions of the gyro could be replaced by a modern flight control system located somewhere within the aircraft's outer mold line. The model was tested in a number of non-rotating configurations, orientations, and tunnel conditions. Baseline results compared favorably with historical drag measurements, and showed approximately a 50% reduction in hub drag with the gyro removed, with an additional 10% reduction due to rudimentary streamlining of the bluff outer hub arm.

Acknowledgments

The authors would like to acknowledge the valuable assistance of Don Morr, Joe Hudson, Robert Mitchell, Frank Harris, Bob Ormiston, Wayne Johnson, Phillip Tanner, Preston Martin, Alex Grima, Jason Cornelius, Nili Gold, Steve Nance, Bruce Gessick, Brian Chan, Chris Silva, Jeff Sinsay, Andrew Gallaher, Alex Moodie, Mark Calvert, and Robert Vocke Jr. This work was made possible through their vision, advice, talent, and feedback.

Contents

List of Figures

List of Tables

List of Symbols

α_c	Corrected angle of attack
α_g	Geometric angle of attack
α_s	Hub shaft angle
$\Delta\alpha_w$	Angle of attack correction due to lift-induced flow-turning
$\Delta\alpha_{up}$	Angle of attack correction due to tunnel up-flow
δ	Boundary correction factor
ϵ_t	Total blockage correction factor
λ	Ratio of tunnel height to tunnel width
λ_T	Taper Ratio
ψ	Hub azimuth
AR	Aspect Ratio
b	Test article geometric span
b_e	Effective span
b_v	Vortex span
C	Tunnel cross section area
C_L	Hub lift coefficient, based on model planform area
C_{LW}	Wing lift coefficient
D	Aerodynamic drag
f_e	Hub flat plate drag area
GW	Gross weight
k	Ratio of model effective span to tunnel jet width
k_{hub}	Empirical hub drag factor
L	Aerodynamic lift
M	Mach number
PM	Aerodynamic pitching moment
q_c	Corrected dynamic pressure
q_u	Uncorrected dynamic pressure
Re	Reynolds number
S_f	Test article frontal area
S_p	Test article planform area
v	Velocity

1. Introduction

A major barrier to efficient high-speed helicopter flight is the drag of the main rotor hub, which can account for up to a third of the entire aircraft drag (Keys and Rosenstein 1978; Reich *et al.* 2016). Hub drag becomes especially critical in the design of high-speed and high-efficiency compound helicopters, which rely on low-drag components to achieve the desired performance (Moodie and Yeo 2012). Unfortunately, there are few examples in the literature of hubs designed primarily to be low-drag (Harris 2012). Figure 1.1 shows historical main hub drag values for various helicopters versus helicopter gross weight. The slanted lines represent constant values of the empirical factor k_{hub}, with the best hubs on record falling near the $k_{hub} = 0.5$ line, where

$$k_{hub} = \frac{f_e}{(GW/1000)^{2/3}}. \tag{1.1}$$

Here, f_e is the hub flat plate equivalent drag in square feet and GW is the gross weight of the helicopter in pounds. Thus, k_{hub} is representative of a classical square-cube relationship of area to weight, where a lower k_{hub} equates to lower hub drag for a given gross weight. Current high-efficiency and high-speed compound designs have assumed future technology will lead to $k_{hub} = 0.35$, which represents a significant improvement over the state-of-the-art (Moodie and Yeo 2012). The justification for these low-drag assumptions has been the AH-56 Cheyenne's novel "door hinge" hub, comprised of a main hub assembly and a mechanical control gyro mounted on top (see Figure 1.2). All of the conventional parts of the Cheyenne hub—mast, fixed hub, movable hub, and tension-torsion pack—present a low frontal area when compared to a conventional rotor hub, and represent a probable lower bound on hub drag following a conventional hub design (Ormiston 2016). All drag data available for the Cheyenne hub is for the combined hub and gyro configuration, and is shown in Figure 1.1, falling just below the $k_{hub} = 1.20$ line. It is reasonable to assume that in a modern version of the Cheyenne-style hub, the feedback and stability control functions of the gyro could be replaced by modern rotor control schemes, leaving just the low frontal area components, and a compelling design for a low-drag hub system. This concept of a low drag Cheyenne-like hub is a major enabler of the current high-efficiency compound designs, and thus it is critical that these assumptions be confirmed with experimental data.

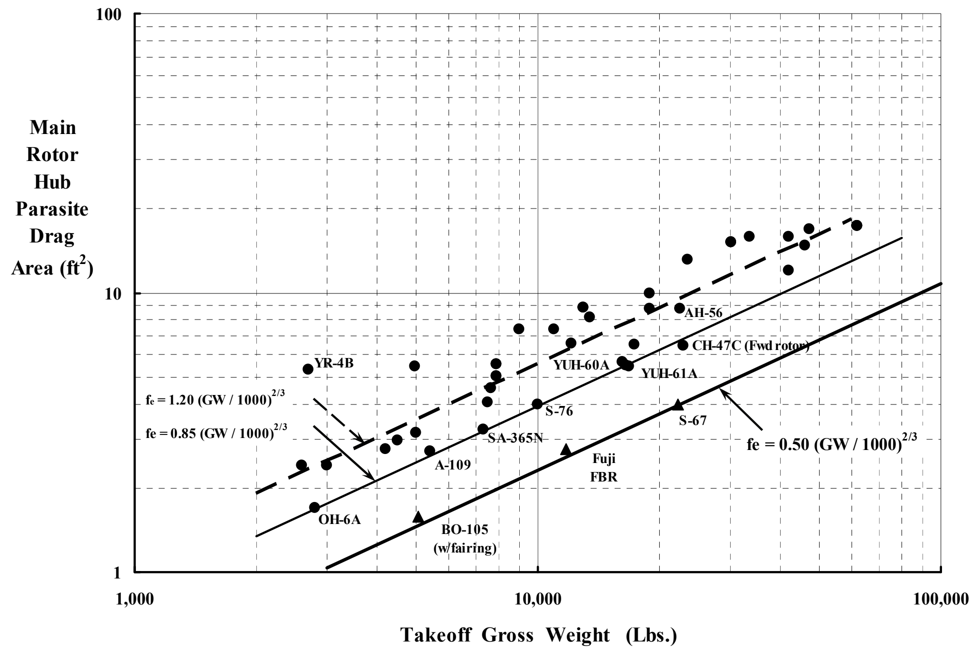

Figure 1.1: Log-log plot of helicopter main rotor hub drag as a function of helicopter gross weight (Harris 2012).

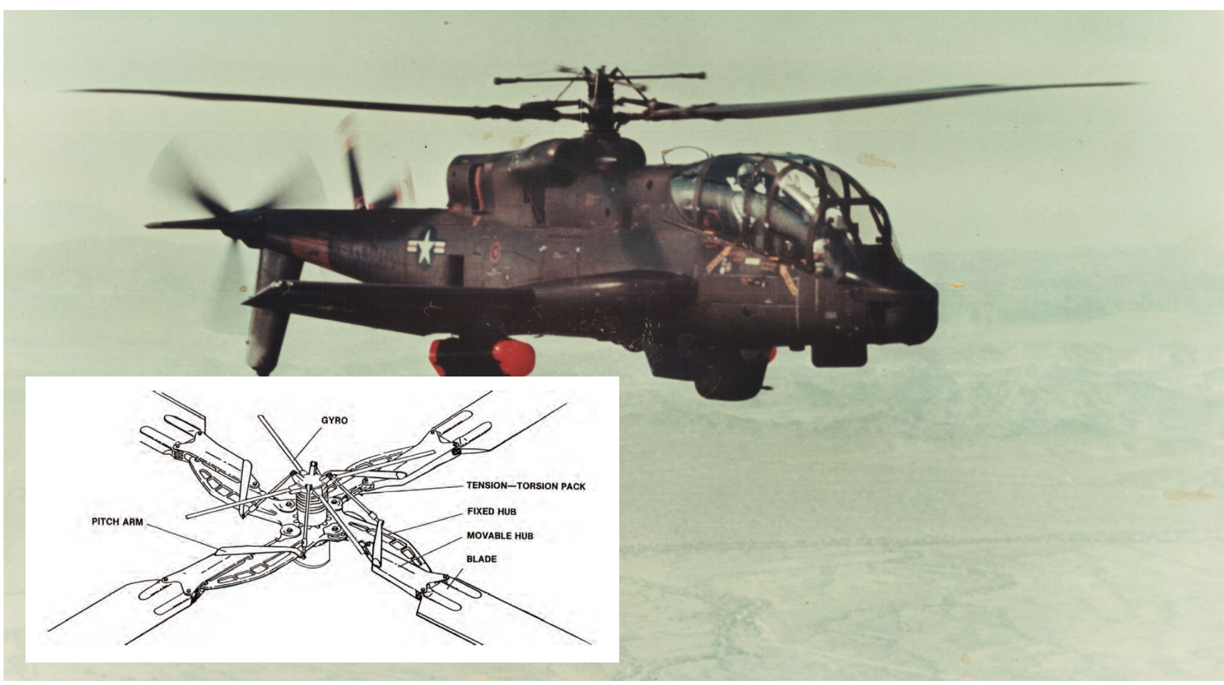

Figure 1.2: The Lockheed AH-56 Cheyenne in flight with the main rotor components called out in the detailed inset. Photo credit: U.S. Army Aviation Museum.

2. Test Description

2.1 Objectives and Scope

The objective of the test was to collect drag build-up data on a 2/5 scale AH-56 hub, both with and without the control gyro installed, and in a faired configuration. Data were collected for a number of discrete build-up configurations, hub azimuth angles, variable angles-of-attack, and over a range of tunnel speeds.

This test was conducted during an approximately three week entry into the U.S. Army 7– by 10–foot wind tunnel at NASA Ames Research Center. The model was non-rotating, and the data were acquired through the tunnel balance system and wind tunnel data system. The maximum free-stream dynamic pressure was approximately 90 $\mathrm{lb/ft^2}$. The model was tested over a shaft angle (equivalent to model pitch) range of $\alpha_s = -2$ to 6 deg. Due to the test's specific focus on both lift- and thrust-compounded rotorcraft, the hub test article was designed without the ability to pitch the blades and thus represents the lowest frontal area (and lowest drag) configuration. This choice is justified because in flight regimes where the low-drag hub becomes desirable (i.e. high-speed flight), a compound rotorcraft's main rotor thrust and lift requirements will be offloaded by auxiliary thrusters and a wing respectively, and the movable hub and rotor blade twist can be designed to allow the hub to operate at low collective settings and shaft angle (angle of attack) at this high-speed operating condition.

2.2 Tunnel and Instrumentation Description

The 7– by 10–foot wind tunnel is a Mach 0.3 subsonic, atmospheric, closed-circuit, single return tunnel with a closed rectangular test section measuring 7 ft wide, 10 ft high and 15 ft long. It is located at the NASA Ames Research Center, Moffett Field, CA and is operated by the U.S. Army Aviation and Missile Research, Development, and Engineering Center.

The tunnel data acquisition system (the Basic Data Acquisition System, or BDAS) manages the collection of atmospheric and load data. BDAS corrects dynamic pressure for atmospheric effects, and resolves the six scale forces into the three forces and moments at a user specified moment center. It also takes into account model pitch and yaw when translating forces and moments to the moment center. Weight and aerodynamic tares can also be applied in real-time, although only weight tares were applied using BDAS during the test.

Table 2.1: 7– by 10–foot wind tunnel scale accuracies, given both in absolute values and percent of full-scale.

Balance Measurement	Scale Accuracy	
Lift	± 0.6 lb	0.01% FS
Side Force	± 1.0 lb	0.03% FS
Drag	± 0.4 lb	0.03% FS
Rolling Moment	± 3.0 ft lb	0.17% FS
Pitching Moment	± 3.5 ft lb	0.19% FS
Yawing Moment	± 6.0 ft lb	0.24% FS

Aerodynamic loads were reacted from the model through an existing test stand (the U.S. Army Rotary Wing Test Stand or RWTS), and into the tunnel metric system. A triangular trailing-edge fairing was added to the cylindrical RWTS strut to reduce load oscillations due to vortex shedding. While the RWTS has an internal balance and the ability to rotate, both of these functions were physically locked out and the test stand was used simply as a strut. Data was sampled at 1024 Hz, and each measurement reported in this work represents 30 seconds of averaged data (no time-history was saved). Additionally, Section 2.2 gives the scale accuracies both in absolute values, and as a percent of the full loading range, for each force and moment measurement.

2.3 Model Description

This work tested a 2/5 scale non-rotating model of the AH-56 Cheyenne hub. A digital CAD model of the hub was created from a combination of historic drawings and physical measurements made on the fifth of ten prototype aircraft built by Lockheed and, as of 2016, was stored at the Army Aviation Museum in Fort Rucker, Alabama. Figure 2.1 shows a CAD rendering of the model, with the major components labeled, while Figure 2.2 shows the model as-built and mounted on the test stand in the tunnel. The model was generally designed to maintain the original hub's outer mold line, even when modifications had been made for manufacturability reasons. For example, the inner 'fixed hub' was broken into five parts—one brown and four yellow parts as shown in Figure 2.1—so it could be more affordably manufactured. Also, the flexible accordion shroud for the gyro support and control structure, which allowed the assembly to tilt, was replaced by a metallic cylindrical gyro standoff tube. Blade stubs were added to limit the effect of the exposed blade grips, although determining the true drag of the hub without blades (but including the influence of the blades) was beyond the scope of this test.

Figure 2.3 gives the major test article dimensions, and explicitly shows the major test variables, ψ (hub azimuth, positive counter-clockwise from the top) and α_s (model shaft angle, positive when the hub is pitched up). The maximum width of the test article is 82 inches and the frontal area of the model in an un-pitched configuration is about 2.5% of the tunnel area (1.72 ft^2). Note that the model is mounted here in a 'cross' configuration, defined in this test as $\psi = 0$ deg. The model moment center, about which all forces and moments were reported, was coincident with the intersection of the test stand azimuthal axis of rotation, and the edgewise centerline of the hub. This centerline was defined as orthogonal to the ψ axis, and 42 in above the tunnel floor at when $\alpha_s = 0$ deg. Thus, the moment center changed as a function of α_s, but was constant with respect to ψ.

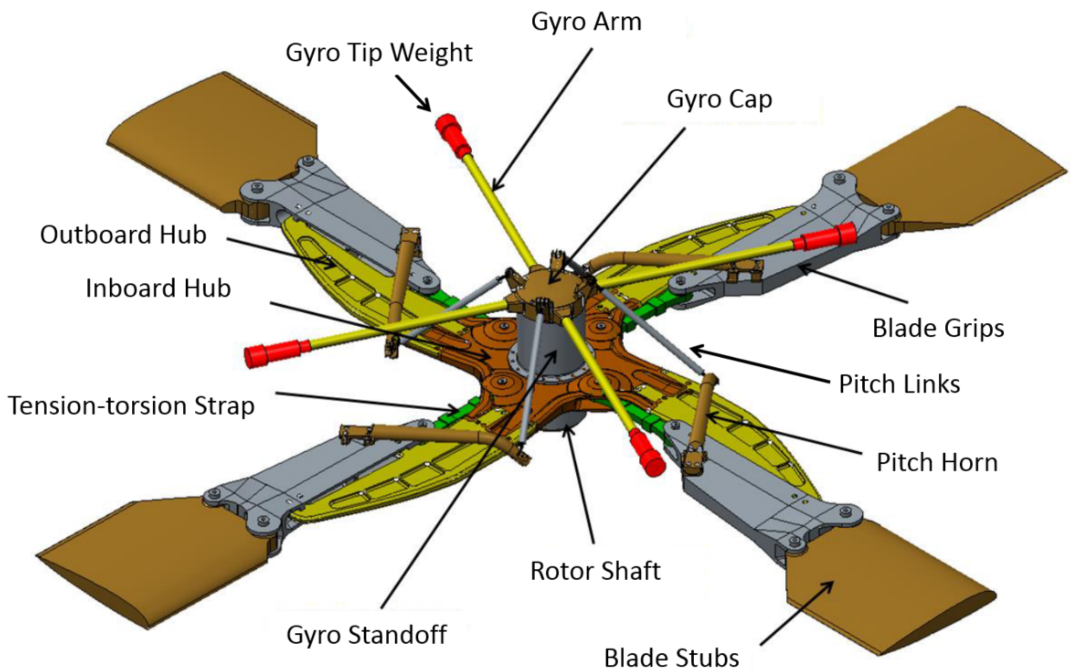

Figure 2.1: 3D CAD representation of the wind tunnel test article

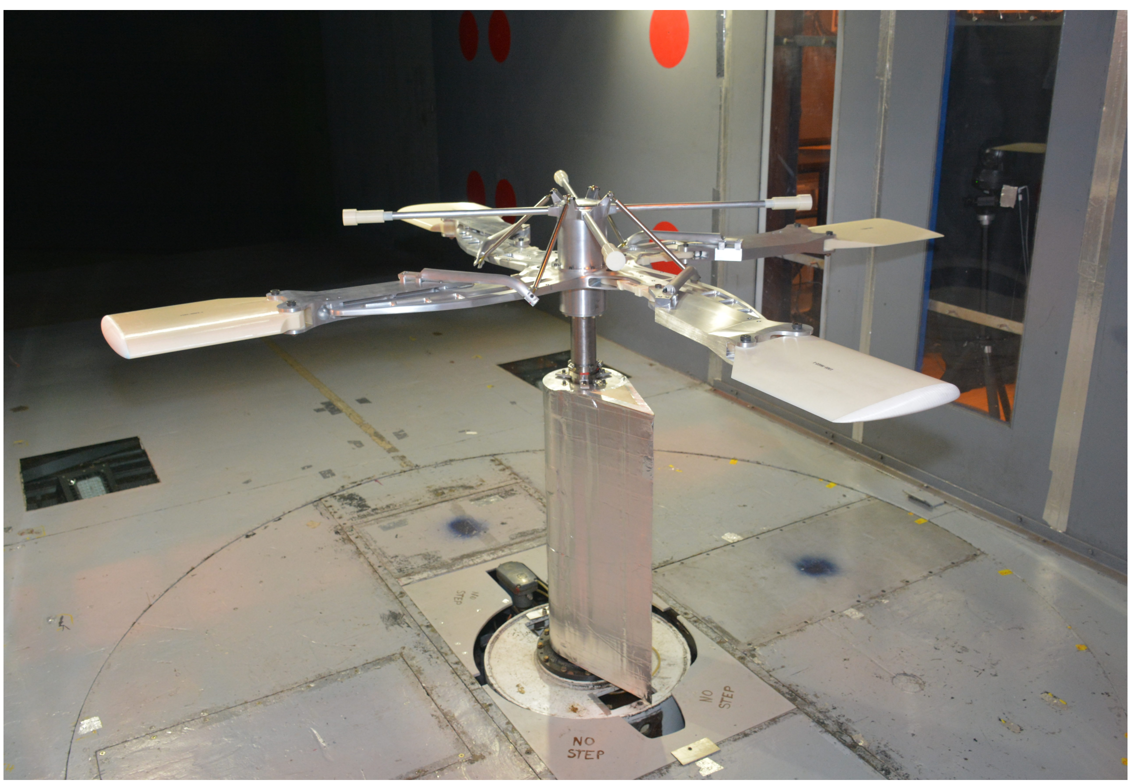

Figure 2.2: The full hub model mounted in the U.S. Army 7– by 10–foot wind tunnel at NASA Ames Research Center

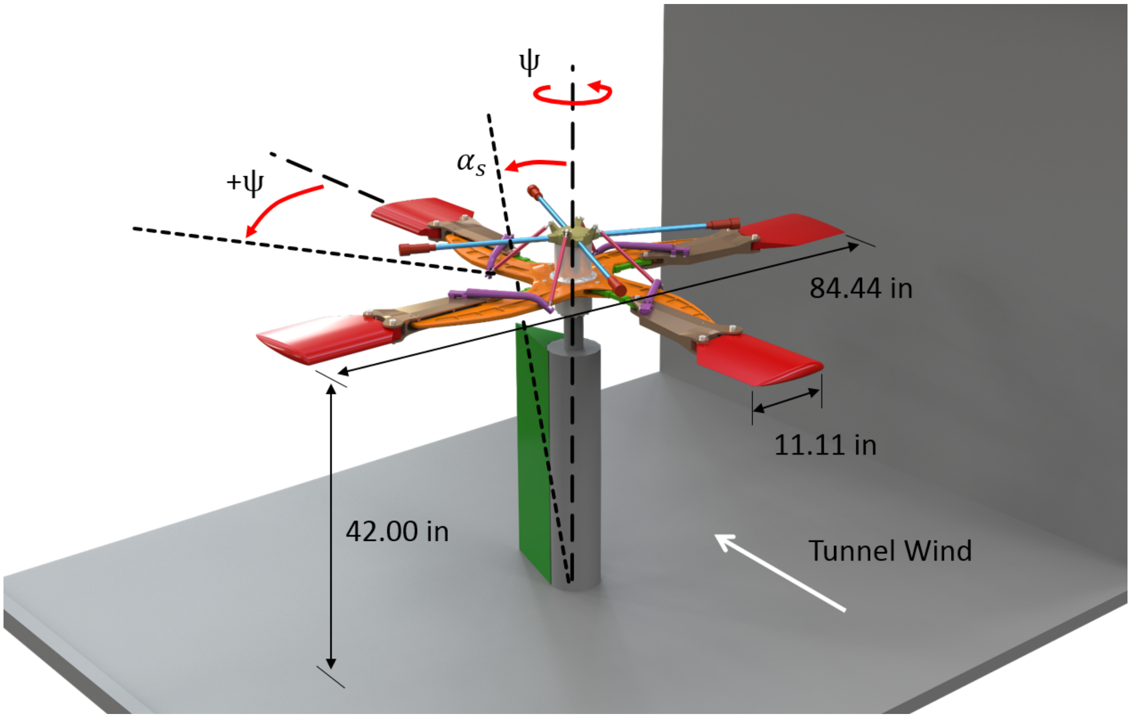

Figure 2.3: Perspective view of the hub mounted in the tunnel at $\psi = 0$ deg with major dimensions and test variables (α_s and ψ) labeled

There were a total of 11 separate hub configurations tested, seven of which (1 to 7) were a drag build-up of the historic hub. Once testing was completed for the historic hub configurations, a simple aerodynamic fairing was designed to streamline some of the more bluff features of the hub, leading to two additional configurations (8 and 9). The last two configurations (10 and 11) had varying amounts of aluminum tape added to the model to smooth out draggy features of the historic hub, and were steps towards the final low-drag faired hub. See Figure 2.4 for a visual summary of the different configurations. Note that in this context, the term fairing—usually understood as an aerodynamic shape fitted over or around an object—refers to material added to provide a generally smooth contour to formerly bluff parts without increasing the hub's frontal area. Figure 2.5 shows a top view of a hub arm, with the leading and trailing edge fairings on the movable hub labeled. The trailing edge fairing was designed by CAD and 3D printed, while the leading edge fairing was hand-cut and shaped out of foam. Both fairings were secured to the existing model using aluminum tape. Figure 2.6 shows a close up of a fully faired arm with a cross-section showing the difference between the faired and un-faired configurations. Figure 2.7 shows the entire faired hub mounted in the tunnel. No attempt was made to analyze or optimize the shape of these fairings, the goal was simply to generally smooth and contour the outer hub. Dimensioned drawings of configurations 4, 6, and 8 are presented in Appendix B.

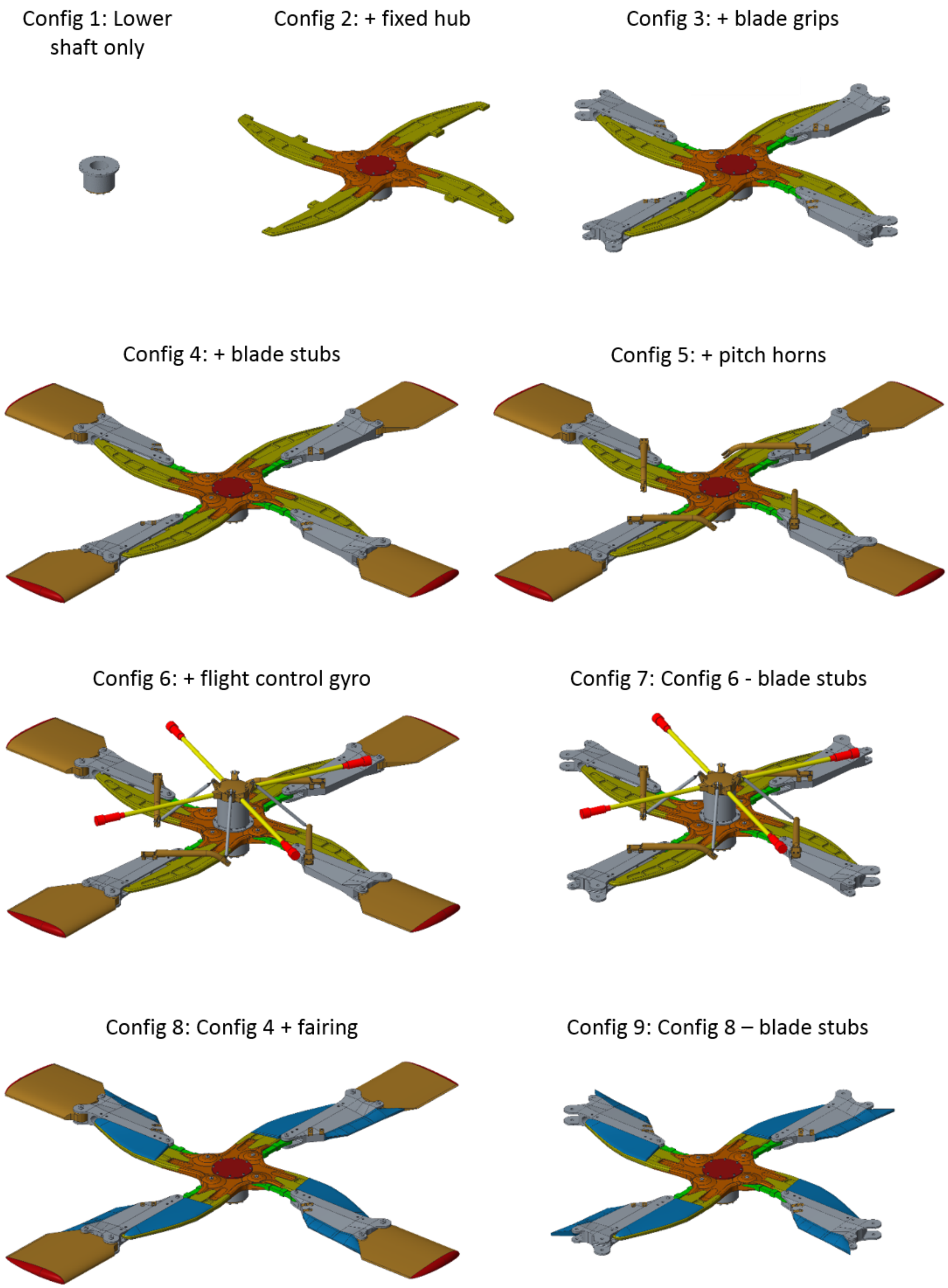

Figure 2.4: CAD renderings of the various hub build up configurations. Of particular interest are Configurations 4, 6, and 8, which represent the "low frontal area", full Cheyenne hub, and faired hub respectively. Not shown are configurations 10–11, which correspond to various stages of aluminum tape additions.

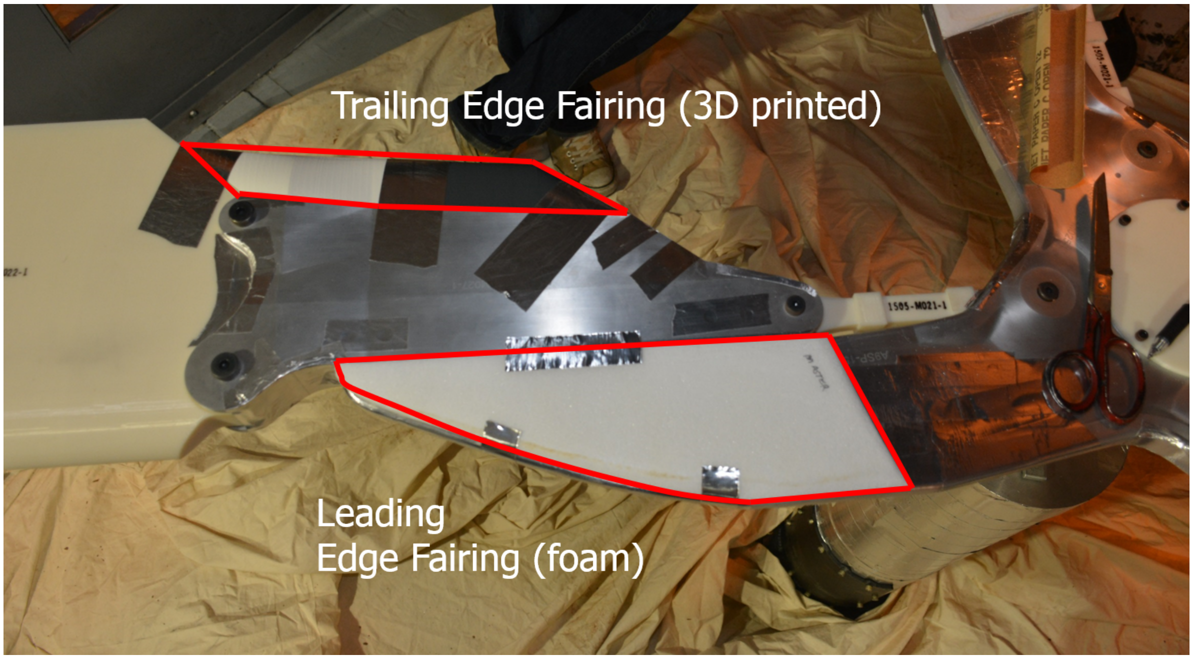

Figure 2.5: The leading edge (foam) and trailing edge (3D printed plastic) fairings before being covered in aluminum tape

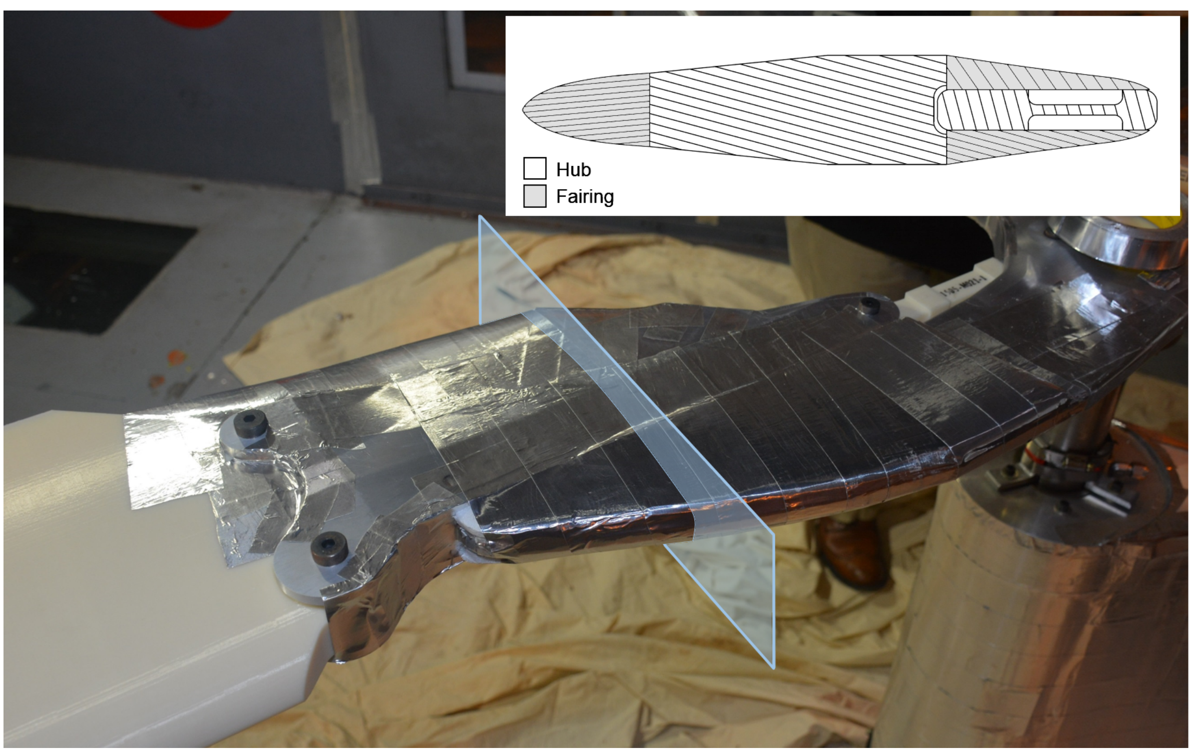

Figure 2.6: Closeup of the final fairing

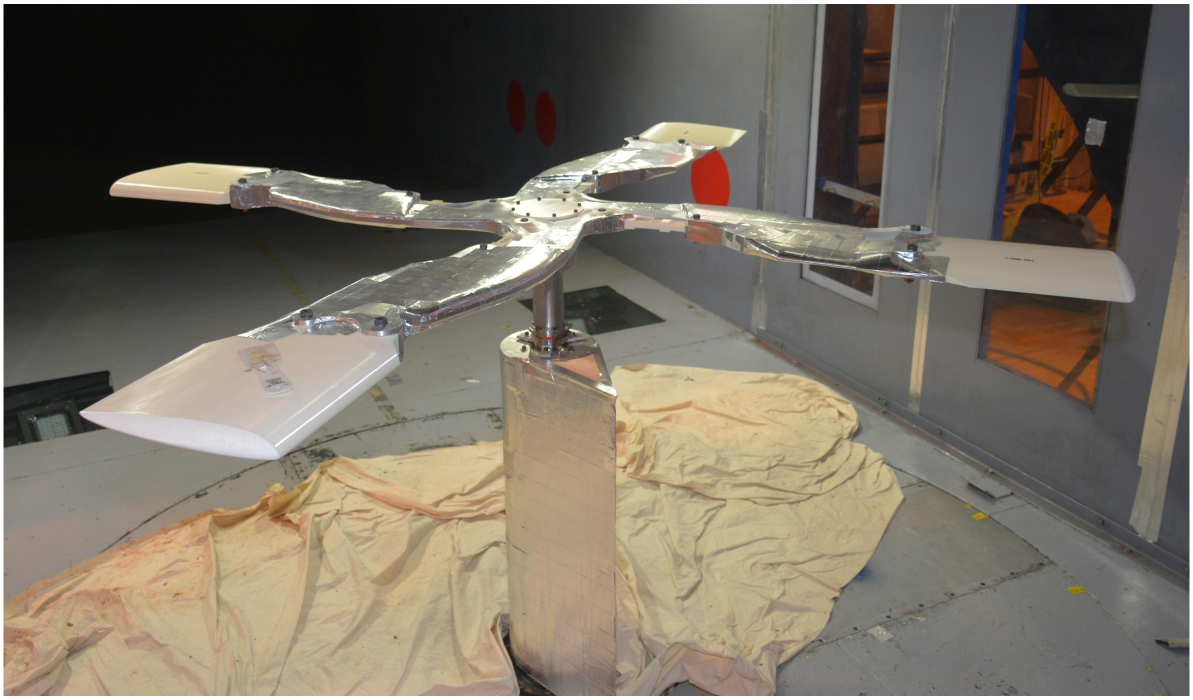

Figure 2.7: The final faired hub (Configuration 8) mounted in the tunnel

2.4 Test Matrix

Table 2.2 summarizes the test matrix and the component build-up for each configuration. Configurations 0 through 6 represent a component build-up of the hub, and were part of the original test plan. Configuration 7 was added for model envelope expansion, and Configurations 8 through 11 represent various stages of fairing of Configuration 4. Isometric views of Configurations 1–9 are given in Figure 2.4. Note that most data were collected at $q_u = 60 \text{ lb/ft}^2$ as the model D/q was determined to be fairly insensitive to Reynolds number over the range tested and 60 lb/ft^2 was a safe dynamic pressure, both for the model and the tunnel. A summary of all collected data corresponding to this test matrix can be found in Tables C.2 to C.12 in Appendix C.

2.5 Test Limitations

2.5.1 Rotation

The choice to do a non-rotating test was driven largely by cost and schedule constraints. Quantifying the effect of hub rotation on measured drag has been the subject of many tests. Keys and Rosenstein (1978) summarize five hub drag tests which compared rotating to non-rotating data (H-21, a rotating horizontal cylinder, HLH, CH-46, and CH-47). Three of these tests showed that rotating a hub increases drag over the maximum non-rotating value somewhere between 5 and 15% , while the other two tests showed that the rotating drag value is within the bounds of the drag found during a static azimuthal sweep. Additionally, Hill and Louis (2012) compared rotating and non-rotating CFD to wind tunnel data

Table 2.2: Summary of the test matrix. Note that the majority of the α_s sweeps were taken at 60 $\mathrm{lb/ft^2}$, and not all combinations of q_u, α_s, and ψ were tested.

Configuration	Description: Rotor Shaft	Fixed Hub	Movable Hub	Blade Stubs	Pitch Horns	Gyro Assembly	Fairing	Aluminum Tape	q_u, $\mathrm{lb/ft^2}$	α_s, deg	ψ, deg
0	*Test Stand Only*								30 60 90	-2 to 6	*Not Applicable*
1	●								30 60 90	-2 to 6	*Not Applicable*
2	●	●							30 60	-2 to 6	0 22.5 45 67.5
3	●	●	●						30 60	-2 to 6	0 22.5 45 67.5
4	●	●	●	●					30 40 50 60 90	-2 to 6	0 22.5 45 67.5
5	●	●	●	●	●				30 60	-2 to 6	0 22.5 45 67.5
6	●	●	●	●	●	●			10 20 30 40 50 60 70	-2 to 6	0 22.5 45 67.5
7	●	●	●		●	●			30 60	-2 to 6	0
8	●	●	●	●			●	●●	30 60 90	-2 to 6	0 22.5 45 67.5
9	●	●	●				●		30 60 90	-2 to 6	0 22.5 45 67.5
10	●	●	●	●				●	30 60	-2 to 6	0 45
11	●	●	●	●				●●	30 60	-2 to 6	0 45

and concluded that rotating hub simulations were unnecessary to make accurate drag predictions. The only sweeping conclusion that can be drawn from these somewhat conflicting studies is that a non-rotating test where azimuth is varied will give an indication of the magnitude of the rotating hub drag value, and that a rotating test is required to obtain the true rotating drag value. Thus data are presented in this study both as a function of azimuthal angle, and also as an averaged value with range bars depicting the upper and lower bounds of the measured drag data, allowing the reader to draw their own conclusions.

2.5.2 Interference Drag

The present work tests the AH-56 hub in isolation, and so no information about mutual hub/pylon drag is available. For reference, Keys and Rosenstein (1978) summarized a number of hub tests where interference drag was investigated, and concluded that mutual hub/pylon interference effects can increase hub drag by 25 to 35%. The range of hub drag numbers available for the AH-56 come from analytical performance models tuned to flight performance data, and it is unclear how interference drag is accounted (Lockheed-California 1972). For the purposes of this test however, comparisons are drawn to the historical data assuming it is reported as isolated hub drag, and that interference effects are accounted elsewhere in the Lockheed performance models.

3. Results and Discussion

3.1 Data Corrections

Data corrections consisted of weight tares, aerodynamic tares, blockage corrections, and wall corrections, applied in that order. No data were available for buoyancy corrections to drag, and so these were neglected. A detailed discussion of the tare and correction methodology can be found in Appendix A. A plot comparing corrected versus uncorrected data is given in Figure 3.1, which shows a maximum change of 5% in both D/q and α_s. A summary of all the uncorrected and corrected data is presented in Appendix C.

3.2 Parasite Drag Variation with Reynolds Number

Figure 3.2 shows the D/q variation with Reynolds number (based on the blade stub chord) for Configuration 6 at a constant $\alpha_s = 0$ deg and $\psi = 0$ deg. The solid line represents a linear fit to the entire data set, and predicts a 0.005 ft^2 increase in D/q per one million increase in Reynolds number. However, the low Reynolds number data appears to be off-trend with the remaining data, perhaps before turbulent transition for a few components. The dashed line represents a linear fit to the data with that point neglected. While there is a small negative slope in the second fit—0.05 ft^2 decrease in D/q per one million increase in Reynolds number—this translates to less than a 5% variation in drag over the tested speed range. The original test plan called for the majority of data to be collected at $q = 90\ \text{lb/ft}^2$ ($Re = 1.6 \times 10^6$), but this study made it clear that testing at a more moderate and safe $q = 60\ \text{lb/ft}^2$ ($Re = 1.3 \times 10^6$) was sufficient.

3.3 Shaft Angle Sweeps

Figures 3.3 to 3.5 show D/q versus shaft angle at $q_u = 60\ \text{lb/ft}^2$ for Configurations 6, 4, and 8 respectively over a range of hub azimuths and shaft angles. The remaining configurations follow similar trends, and are not shown here. Each marker represents an individual data point, and the dashed lines represent constant values of ψ connecting the averaged D/q value at a given ψ and α_s pairing. For all configurations, drag generally follows changes in the model frontal area due to azimuthal rotation and shaft tilt (see Table A.6 in Appendix A for a summary of frontal area values). The full-hub configuration (Figure 3.3) has both the highest drag, and the highest variation in drag with respect to both shaft angle and azimuth. There is an noticeable grouping of the $\psi = 0$ and 22.5 deg and the $\psi = 45$ and 67.5 deg lines

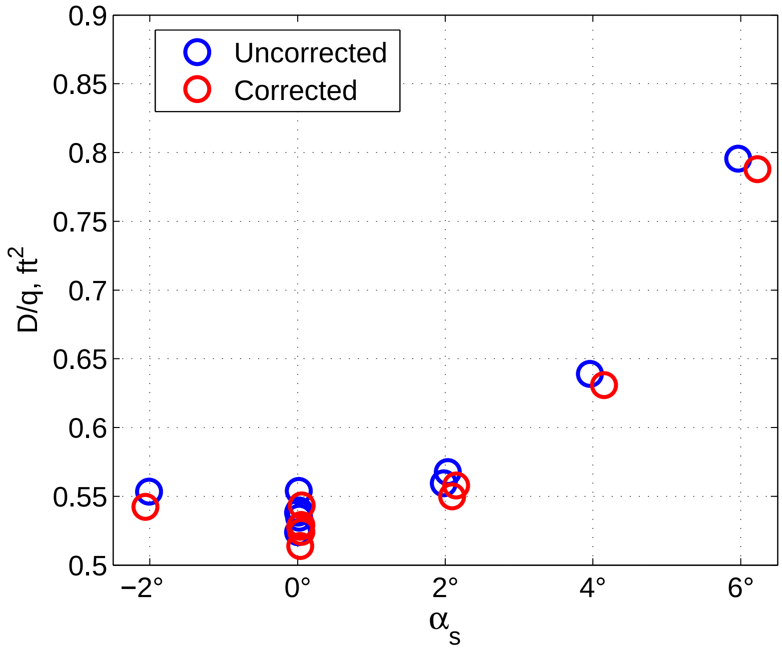

Figure 3.1: Example of the worst case (largest magnitude) data corrections, showing both D/q and α_s changes on the order of 5% for Configuration 8

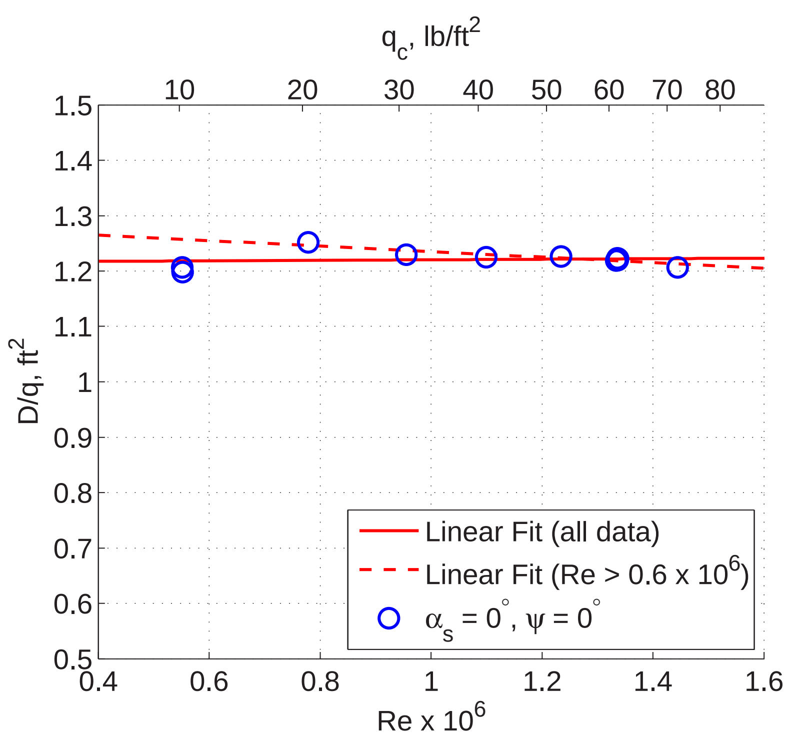

Figure 3.2: Variation of D/q with Reynolds number (Configuration 6, $\alpha_s = 0$ deg, $\psi = 0$ deg)

not present in the other two configurations. Removal of the gyro control system (Figure 3.4) leads to both an overall drag decrease, and a decrease in the variation in drag as a function shaft angle and azimuth. The introduction of the aerodynamic fairing in Configuration 8 (Figure 3.5) continues this trend.

Figure 3.6 shows a summary of the entire drag build-up as noted for each configuration change. For a visual representation of this progression, see Figure 2.4. To simplify the data presentation, these curves represent data averaged over ψ at each discrete shaft angle for each configuration. In general, as components are added to the model, drag increases, with the largest and more bluff components—such as the fixed hub and gyro assembly—contributing the most to total drag. As shown, the gyro represents a third of the entire hub drag, which is consistent with a roughly 30% increase in frontal area from Configuration 5 to 6. When the leading and trailing edge fairings are added however, drag decreases by 20%. This is shown more clearly in Figure 3.7, which also includes range bars for each test point to indicate the lower and upper bounds of the averaged azimuthal sweep drag data. Note that the variation in drag due to azimuthal changes is small compared to the overall drag magnitude. Also, simply removing the gyro and pitch horns decreases drag by about 50% at the minimum drag condition. A final 10% reduction, for an overall 60%, is realized through introduction of the fairing. Recall that the goal of adding the fairing was to reduce form drag by smoothing out the more bluff hub shapes without increasing the hub frontal area. This modification was moderately successful in the present work, considering no aerodynamic analysis was done on the shape beforehand. A clean-sheet door-hinge hub design focusing on drag reduction could likely see additional improvements (Ormiston 2016).

3.4 Azimuthal Sweeps

This section presents the hub drag from Section 3.3 as a function of hub azimuth, ψ. Figures 3.8 to 3.10 show D/q versus azimuth at $q_u = 60\ \mathrm{lb/ft^2}$ for Configurations 6, 4, and 8 respectively. Each marker is an individual datum, and the dashed lines represent constant values of α_s connecting the averaged D/q value at a given ψ and α_s combination. Due to symmetry, $\psi = 90\ \mathrm{deg}$ is equivalent to $\psi = 0\ \mathrm{deg}$ and so in these plots, D/q measured at $\psi = 0\ \mathrm{deg}$ is replotted at $\psi = 90\ \mathrm{deg}$ to give a sense of the data's periodicity. Drag for Configurations 6 and 4 in (Figures 3.8 and 3.9) general decreases as a function of ψ until the minimum frontal area condition is reached, at which point it begins to increase again. In contrast, the faired Configuration 8 (Figure 3.10) shows a pronounced "W" shape, with drag increasing at $\psi = 45\ \mathrm{deg}$ which is the nominal lowest frontal area orientation. A possible explanation for this is proportionally larger interference effects between the front and rear hub arms in this configuration due to addition of the fairing (smoother flow that for the other more bluff configurations). Finally, the drag increase between the $\alpha_s = 0$ and $\alpha_s = 2$ (or -2) deg lines is proportionally much less than between the 2–4 and 4–6 deg increments when contrasted with the frontal area, which changes essentially linearly with α_s in this small-angle region. This suggests that—for this style of hub—thrust compounding, allowing the hub to operate at near-zero shaft angles, is necessary for low-drag operation in high-speed flight. Results from the previous figures are summarized in Figure 3.11, which shows both the minimum ($\alpha_s = 0\ \mathrm{deg}$) and maximum ($\alpha_s = 6\ \mathrm{deg}$) drag for each configuration as a function of ψ. These data like that in Figure 3.7, make it clear that drag is much more sensitive to hub shaft angle than hub azimuth.

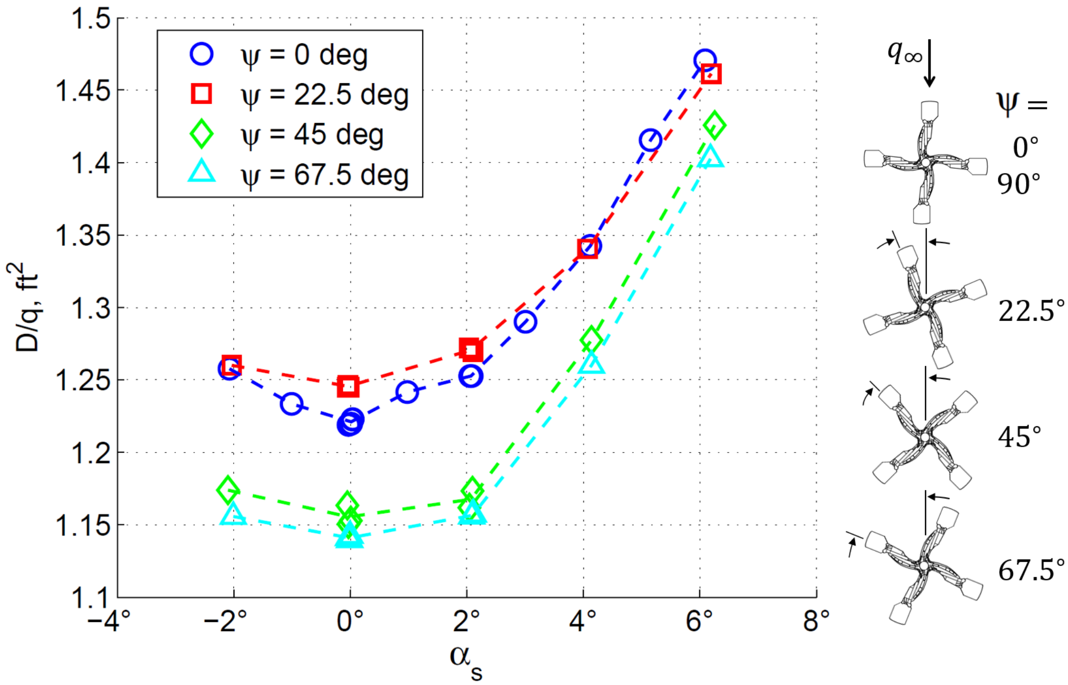

Figure 3.3: D/q versus α_s for Configuration 6 (Config. 4 + pitch horns and gyro). Markers represent data points, and the dotted lines connect the averaged data for each α_s and ψ combination.

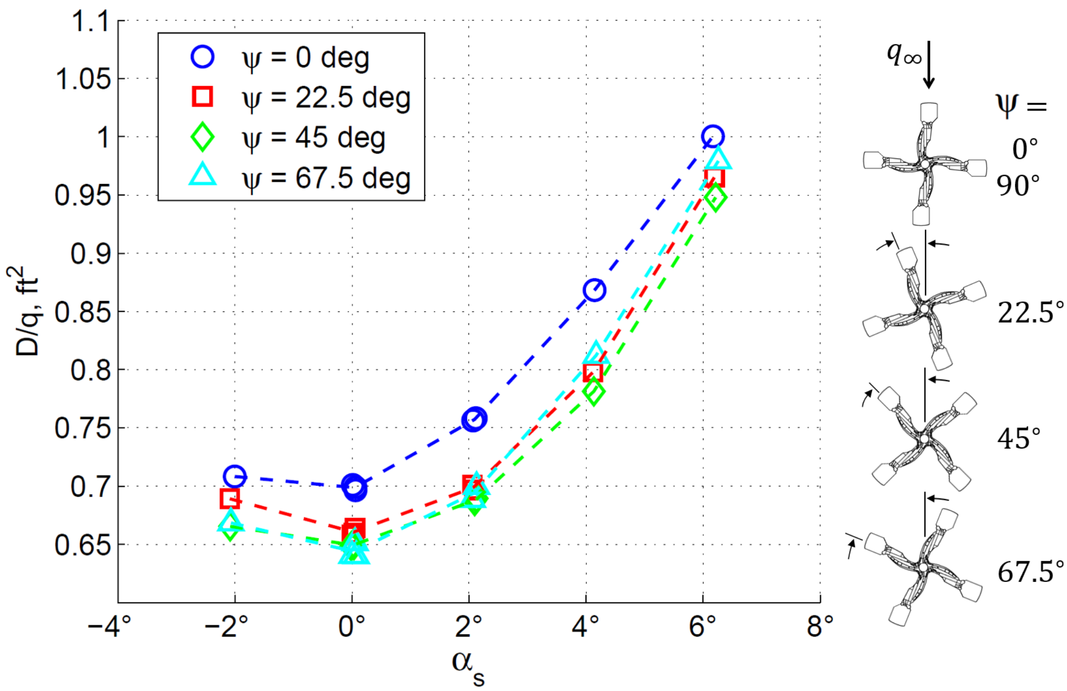

Figure 3.4: D/q versus α_s for Configuration 4 (hub + blades). Markers represent data points, and the dotted lines connect the averaged data for each α_s and ψ combination.

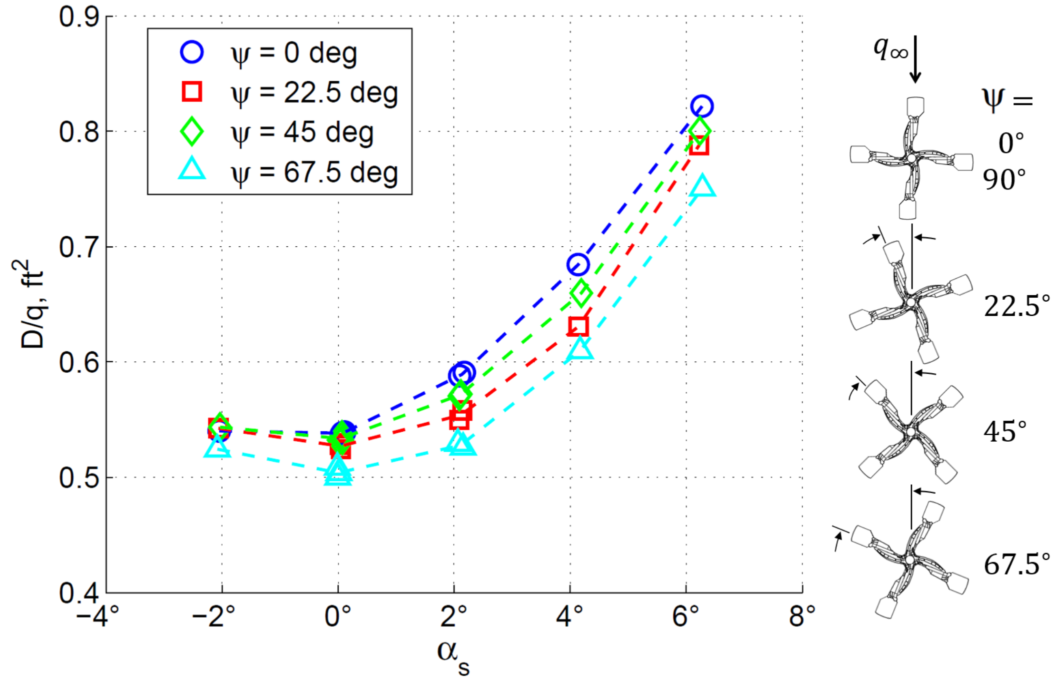

Figure 3.5: D/q versus α_s for Configuration 8 (Config. 4 + fairing). Markers represent data points, and the dotted lines connect the averaged data for each α_s and ψ combination.

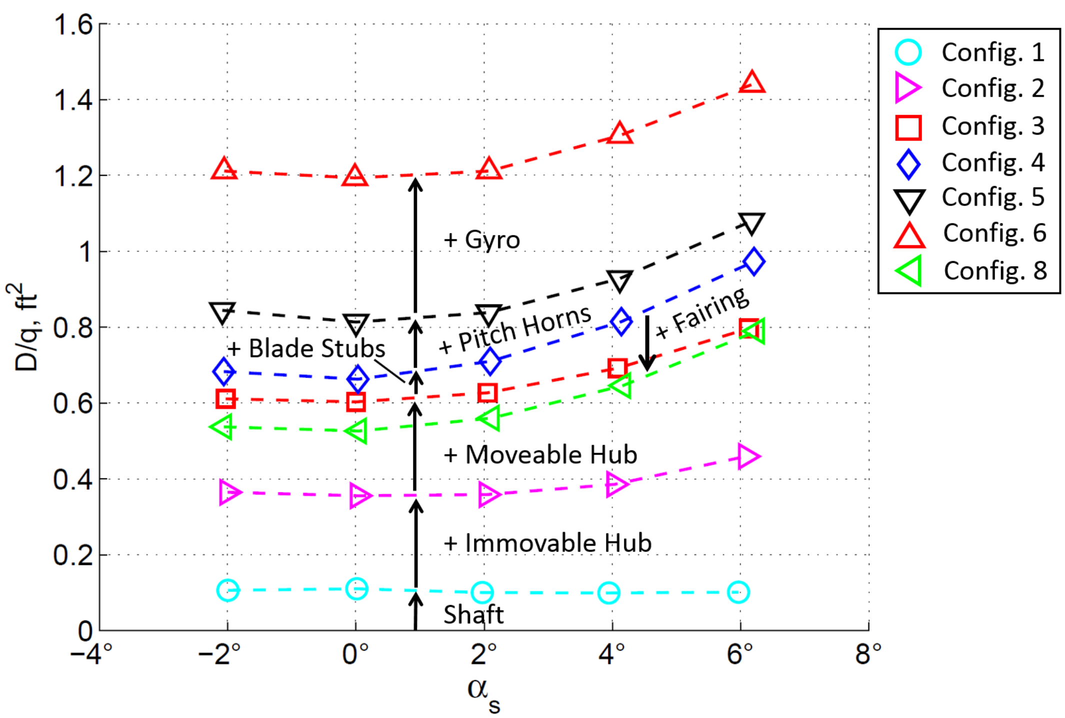

Figure 3.6: D/q averaged over ψ versus α_s at $q_u = 60$ lb/ft^2 for the built-up hub

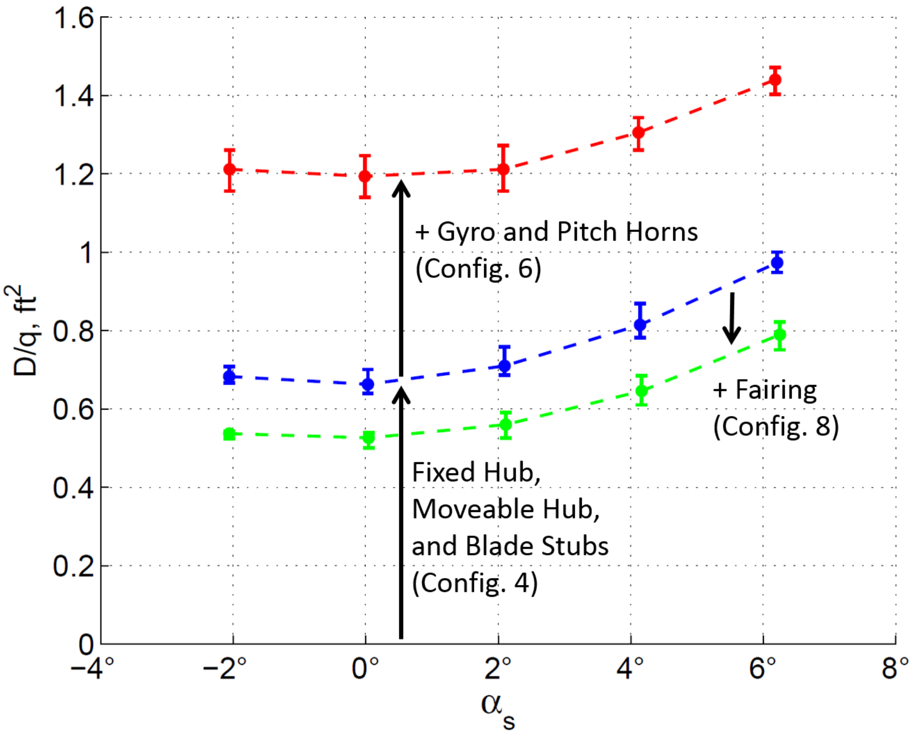

Figure 3.7: D/q averaged over ψ versus α_s for Configurations 4, 6, and 8 at $q_u = 60$ lb/ft^2. The range bars represent the upper and lower limits of D/q with ψ at each averaged point.

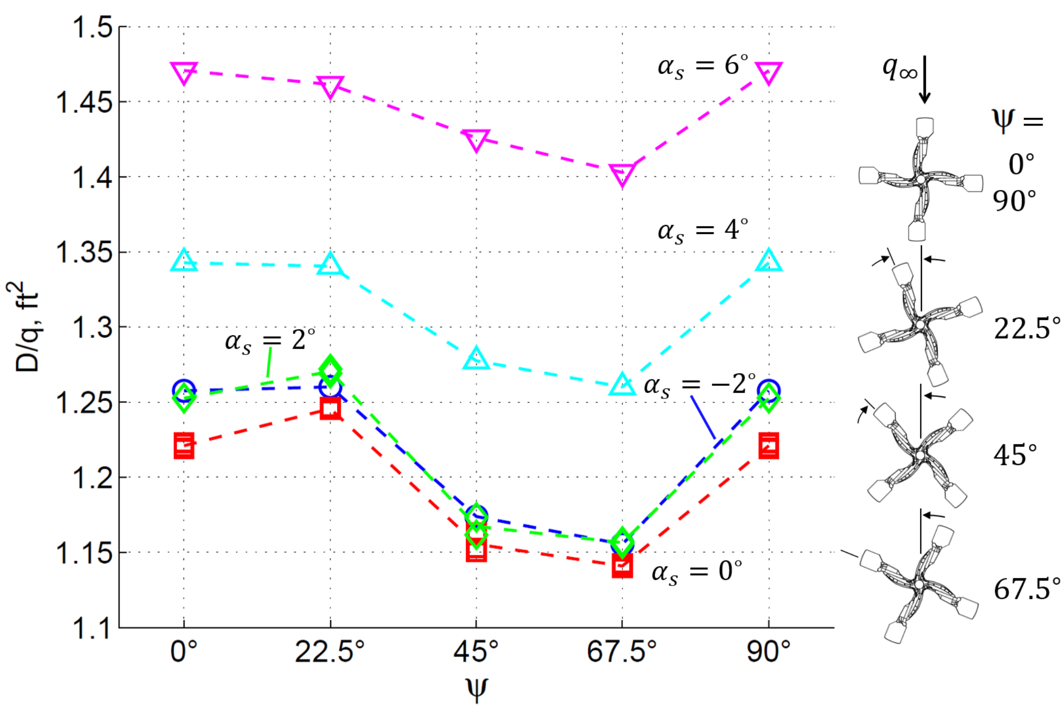

Figure 3.8: D/q versus ψ for Configuration 6 (Config. 4 + pitch horns and gyro). Markers represent data points, and the dotted lines connect the averaged data for each α_s and ψ combination.

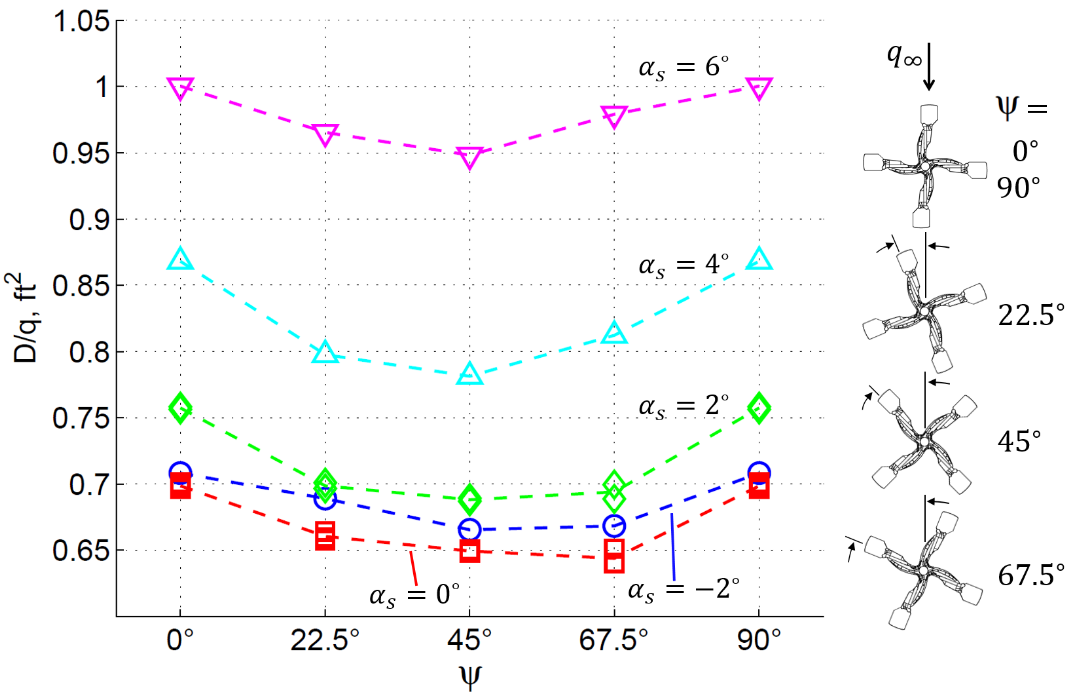

Figure 3.9: D/q versus ψ for Configuration 4 (hub + blades). Markers represent data points, and the dotted lines connect the averaged data for each α_s and ψ combination.

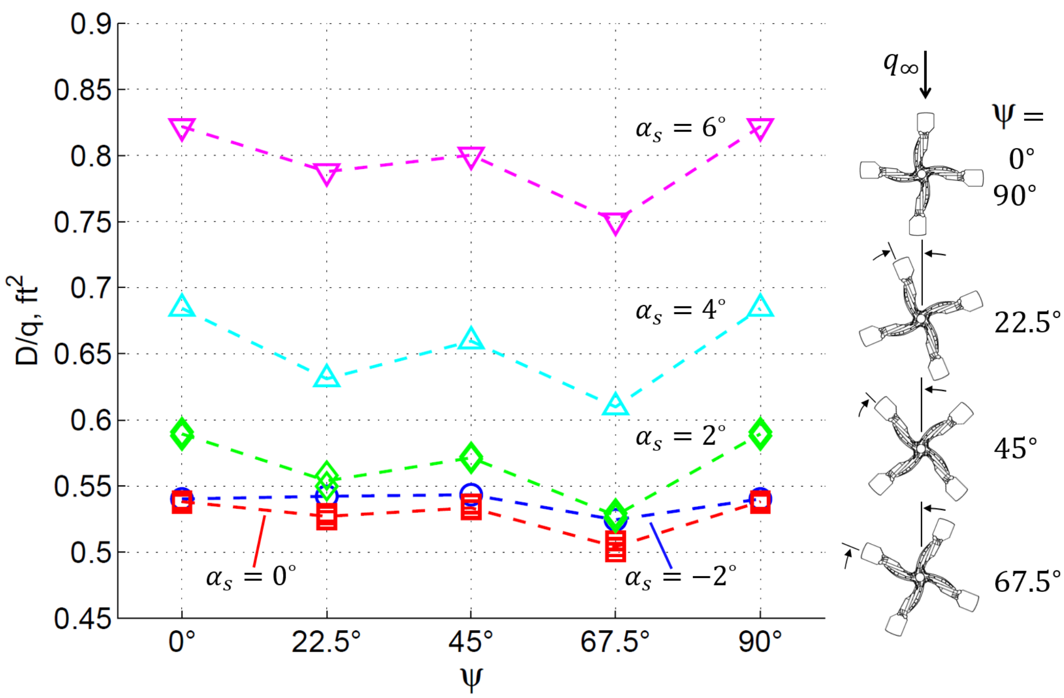

Figure 3.10: D/q versus ψ for Configuration 8 (Config. 4 + fairing). Markers represent data points, and the dotted lines connect the averaged data for each α_s and ψ combination.

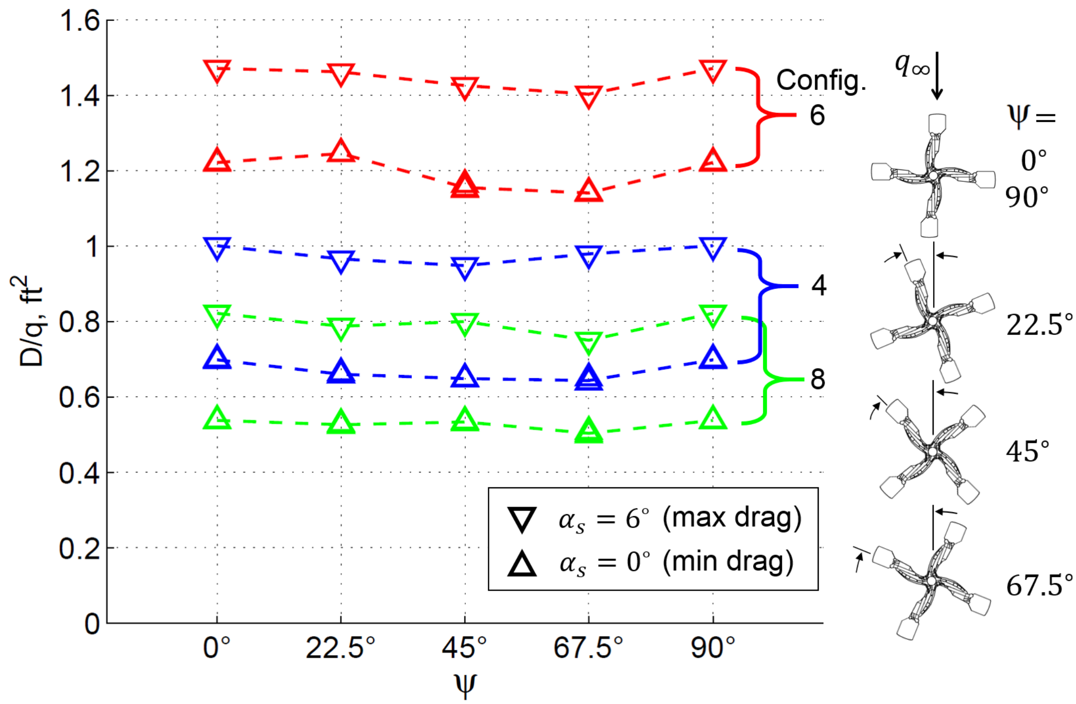

Figure 3.11: D/q versus ψ for Configurations 4, 6, and 8 at $q_u = 60$ lb/ft^2, and at $\alpha_s = 0$ and 6 deg. The values of α_s represent the minimum and maximum drag shaft angles respectively.

3.5 Comparison to Historical Data

Finally, it is interesting to compare the results of this test to the historical data presented in Figure 1.1, to find if any meaningful reduction in drag is, in fact, achieved. To accomplish this, the minimum averaged D/q for each configuration was scaled up to the full-sized aircraft values (neglecting any variation with Reynolds number), converted to a k_{hub} value, and plotted at the AH-56's maximum takeoff gross weight of 22,500 lb. Figure 3.12 presents these results for the three most relevant configurations tested. The full hub, as tested, falls roughly 1.4 ft^2 (15%) below the historic empirical value. This difference could arise from inaccuracy in the historic value (which was not substantiated by wind tunnel testing), inaccuracy of the wind tunnel model geometry, effects of rotation, effects of scaling, unaccounted interference drag, or a number of other sources. Removing the gyro shifts the tested drag down to the $k_{hub} = 0.5$ trend, which represents the best that has been achieved historically. Finally, applying the fairing further decreases the drag to $k_{hub} = 0.41$, about half way to the $k_{hub} = 0.35$ line which represents the Moodie and Yeo (2012) hypothesis of future hub drag technology.

Figure 3.13 shows a close-up of the same data with additional constant k_{hub} lines. The first line, at $k_{hub} = 0.2$, has been suggested by Ormiston (2016) as a stretch-goal for future low drag hub design. This estimation is based generally on the door-hinge concept, with the idealized assumption of a very careful aerodynamic design with component drags similar to thin-airfoil values. The logical extreme of this approach is shown with the $k_{hub} = 0.11$ line, which represents the skin friction drag of a fully turbulent flat plate at $Re = 1 \times 10^6$ (Hoerner 1965) with the wetted area of the full

AH-56A hub. The difference between this lower bound and all of the points above is an indication of the sometimes excessive form drag. As noted in Section 2.3, the fairing used in this test was *ad hoc*, and no attempt was made to optimize it for drag reduction. Thus, an obvious extension to this work is an optimization of the aerodynamic shape of the hub to reduce the form drag, moving the design closer to the proposed goals.

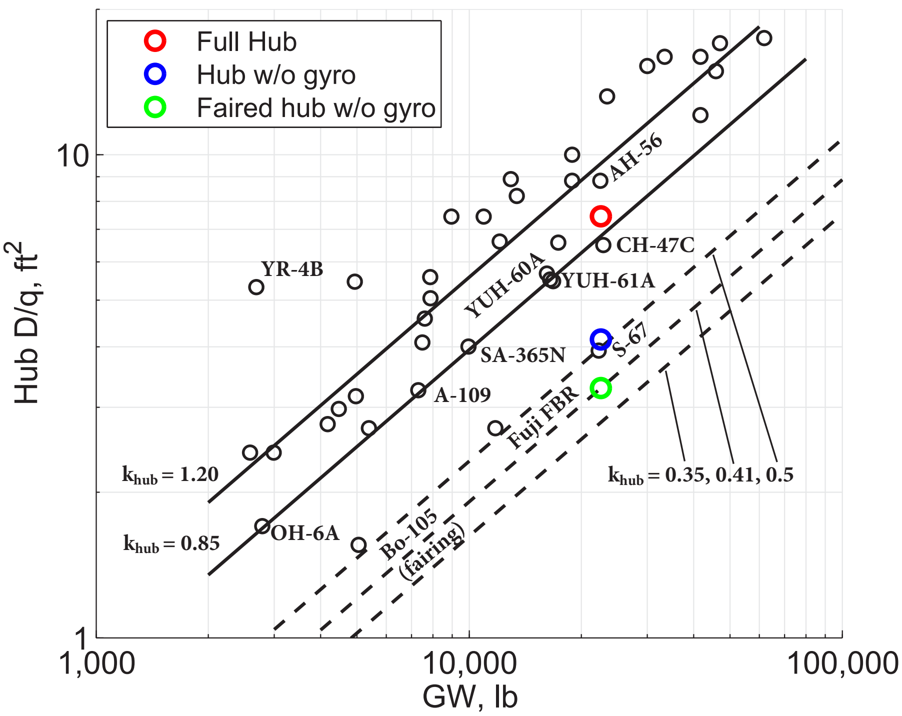

Figure 3.12: Comparison of wind tunnel test data with historical hub drag values plotted on a log-log scale of Hub D/q vs GW

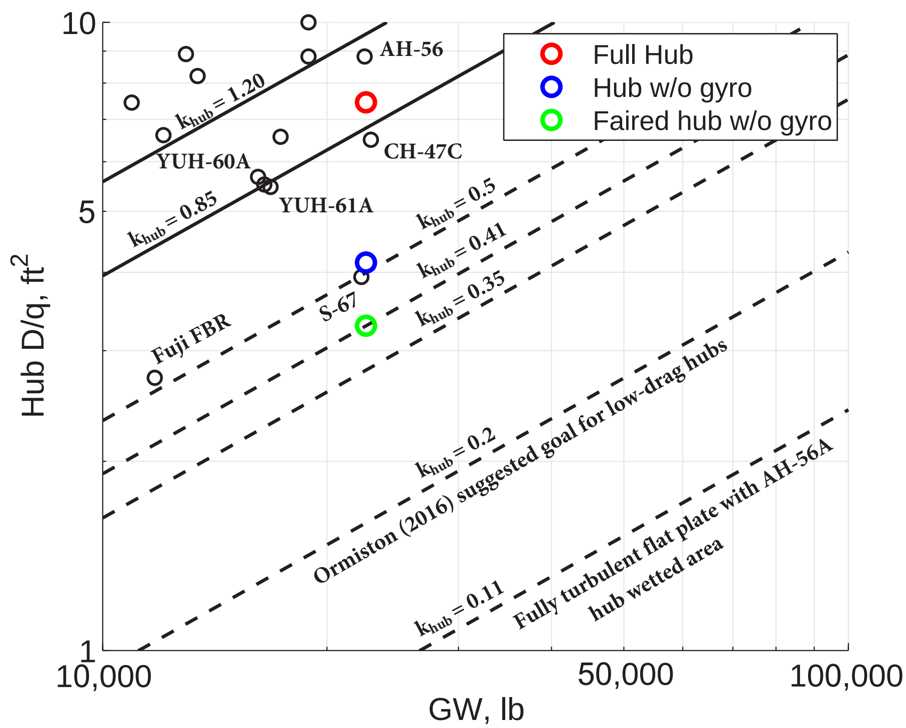

Figure 3.13: Closeup of Figure 3.12 with additional low-drag hub goals plotted on a log-log scale of Hub D/q vs GW

4. Conclusion

A 2/5 scale AH-56 Cheyenne door-hinge style hub was tested in the U.S. Army run 7– by 10–foot wind tunnel at NASA Ames Research Center to quantify the drag of a realistic low-drag hub design. The hub was tested in a number of configurations, azimuths, and shaft angles. The measured drag for the full hub was generally consistent with historical data, and removing the gyro and pitch horns decreased hub drag by approximately 50% at the minimum drag conditions. Additionally, a simple aerodynamic fairing attached to the bluff outer portions of the hub further reduced drag by 10%, resulting in an overall 60% reduction in drag. This put the final faired hub at drag levels far below the current state-of-the-art, but still short of future technology expectations. The remaining gap could possibly be closed through a rigorous aerodynamic design of the door-hinge hub concept, focusing specifically on drag reduction. This future work would also benefit from consideration of the blade control method, rotation, and interference.

References

Barlow, Jewel B., William H. Rae, and Allan Pope (1999). *Low-Speed Wind Tunnel Testing*. 3rd ed. New York: John Wiley & Sons, Inc.

Harris, Franklin D. (2012). *Introduction to Autogyros, Helicopters, and Other V/STOL Aircraft Volume II: Helicopters*. Tech. rep. SP–2012-215959 Vol II. NASA.

Hill, Matthew J and Matthew E Louis (2012). "Rotating Hub Drag Prediction Methodology". *Proceedings of the American Helicopter Society Specialists' Conference on Future Vertical Lift Aircraft Design*. San Francisco, CA.

Hoerner, Sighard. F. (1965). *Fluid-Dynamic Drag*. 2nd ed. Bakersfield, CA: Self published.

Keys, C. N. and H. J. Rosenstein (1978). *Summary of Rotor Hub Drag Data*. Tech. rep. CR-12080. NASA.

Lockheed-California (1972). *Substantiation Technical Data, AH-56 Attack Helicopter*. Tech. rep. LR 25271.

Moodie, Alex M. and Hyeonsoo Yeo (2012). "Design of a Cruise-Efficient Compound Helicopter". *Journal of the American Helicopter Society* 57.3. DOI: `10.4050/JAHS.57.032004`.

Ormiston, Robert A (2016). "Revitalizing Advanced Rotorcraft Research—and the Compound Helicopter: 35th AHS Alexander A. Nikolsky Honorary Lecture". *Journal Of The American Helicopter Society* 61.1. DOI: `10.4050/JAHS.61.011001`.

Reich, David *et al.* (2016). "A Review of 60 Years of Rotor Hub Drag and Wake Physics: 1954–2014". *Journal of the American Helicopter Society* 61.2. DOI: `10.4050/JAHS.61.022007`.

Appendix A. Tares and Data Corrections

A.1 Weight and Aerodynamic Tares

A wind-off pitch sweep was conducted for each configuration and pitch moment tares as a function of α_s were calculated in the tunnel data acquisition system. These tares were applied as data were collected for each configuration as appropriate. A wind-off zero point was taken at the beginning of each run, thereby eliminating the need for lift or drag weight tares were required. While the model azimuth was adjusted during testing, the tunnel balance system was never yawed, and so no yaw weight tare corrections for force or moment data were necessary.

Aerodynamic tares were taken from the Configuration 0 (test stand only) runs. This included pitch sweeps over the entire test stand range at uncorrected dynamic pressures of 30, 60, and 90 $\mathrm{lb/ft^2}$. While data were collected for all six forces and moments, aero tare models were only developed for lift, drag, and pitching moment measurements. In each case, a polynomial was fit to the test data as a function of α_s, at a given tunnel dynamic pressure. The tare data and corresponding fits for drag, lift, and pitching moment are shown in Figures A.1 to A.3. Polynomial order was chosen in each case to produce a fit that most closely fit the data. The coefficients for these fits are given in Tables A.1 to A.3. Additionally, data was recorded at $\alpha_s = 0\ \mathrm{deg}$ for dynamic pressures other than the 30, 60, and 90. An additional aerodynamic tare was then also developed for lift, drag, and pitching moment as a function of q_u for this special case (presented in Table A.4).

A.2 Blockage Corrections

Due to the complex and bluff shape of the test article, a separate analysis of solid and wake blockage was not considered. Instead, the approximate blockage correction factor suggested in Barlow, Rae, and Pope (1999) was used. This correction factor is defined as

$$\epsilon_t = \frac{1}{4}\frac{S_f}{C} \tag{A.1}$$

where S_f is the model frontal area and C is the test section cross sectional area. The final blockage correction is then defined as

$$q_c = q_u \left(1 + \epsilon_t\right)^2 \tag{A.2}$$

$$v_c = v_u (1 + \epsilon_t) \tag{A.3}$$

where q is dynamic pressure and v is velocity, and the subscripts c and u represent the corrected and uncorrected values respectively. Model frontal area depended on orientation, and a separate blockage calculation was made for each combination of configuration, and azimuth, and at $\alpha_s = -2, 0, 2, 4$ and 6 deg. These values are given in Table A.5 along with the calculated correction factor. Occasionally, data were taken at shaft angles other than the five given above. For these cases, the frontal area was interpolated using a piecewise cubic Hermite interpolating polynomial calculated in MATLAB using the `pchip` function. For configurations of interest, tunnel blockage (including the test stand) varied from 3.5 to 6%, corresponding to a 2 to 3% increase in dynamic pressure.

A.3 Wall Corrections

Although the hub is largely a bluff body, in the more streamlined configurations it generated up to 170 lb of lift, corresponding to a C_L of about 0.3 (based on model planform area). While this is not a significant amount of lift, it translates in the worst case to a 5% correction in α_s and 2% correction in drag, and so the corrections were calculated for all data points. No wall corrections were made to Configurations 0 and 1 (test stand and shaft), or to the lift and pitching moment data for all configurations.

The angle of attack correction is given as

$$\alpha_c = \alpha_g + \Delta\alpha_{up} + \Delta\alpha_w \tag{A.4}$$

where α_g is the geometric angle of attack, $\Delta\alpha_{up}$ is the tunnel up-flow, and $\Delta\alpha_w$ is defined, in radians, as

$$\Delta\alpha_w = \frac{\delta S_p}{C} C_{LW}. \tag{A.5}$$

Here, δ is the boundary correction factor, S_p is the test article planform area, C is again the tunnel cross sectional area, and C_{LW} is the "wing" lift coefficient. Expanding C_{LW} produces the more convenient expression

$$\Delta\alpha_w = \frac{\delta}{C}\frac{L}{q_c}. \tag{A.6}$$

There was insufficient information available about the tunnel to evaluate $\Delta\alpha_{up}$, and so this term was neglected. For calculation of the boundary correction factor δ, the hub was treated as a wing with a chord equal to the blade stub chord, and a planform area of the configuration in question. These assumptions were used to calculate the ratio of effective span to vortex span, b_v, using Figure A.5 and then to calculate the effective span,

$$b_e = \frac{b + b_v}{2}. \tag{A.7}$$

The effective span was used to calculate δ with Figure A.4. Here, the jet width is 10 ft, and λ is the ratio of tunnel height to width, 0.7 in this case. The value of δ was calculated for every configuration and orientation as b_e varied, and averaged to about 0.12. Table A.7 gives the values of b used for these wall correction calculations, and also S_p for reference.

The drag correction is given as

$$C_{Dc} = C_{Du} + \Delta C_{D,up} + \Delta C_{Dw} \tag{A.8}$$

where C_{Du} is the drag coefficient with weight and aerodynamic tares applied. $\Delta C_{D,up}$ was neglected as described in the preceding paragraph. The drag due to the wall corrections is defined as

$$\Delta C_{Dw} = C_{LW} \Delta\alpha_w = \frac{\delta S_p}{C} C_{LW}^2 \tag{A.9}$$

with δ defined as above. Again, expanding the coefficients leads to the convenient form

$$\left(\frac{D}{q_c}\right)_c = \left(\frac{D}{q_c}\right)_u + \frac{\delta}{C}\left(\frac{L}{q_c}\right)^2. \tag{A.10}$$

Table A.1: Coefficients for the drag tare polynomials in the form $D_{tare} = P_1\alpha_{s,u}^3 + P_2\alpha_{s,u}^2 + P_3\alpha_{s,u} + P_4$, where D_{tare} has units of lb and $\alpha_{s,u}$ is in degrees.

$q_u, \mathrm{lb/ft}^2$	P_1	P_2	P_3	P_4
30	1.1469×10^{-2}	3.9571×10^{-3}	1.3054×10^{-1}	2.3327×10^{1}
60	1.0696×10^{-2}	2.2233×10^{-2}	5.1744×10^{-1}	4.8684×10^{1}
90	-2.2224×10^{-3}	-3.7826×10^{-3}	1.4076	7.6844×10^{1}

Table A.2: Coefficients for the lift tare polynomials of the form $L_{tare} = P_1\alpha_{s,u}^3 + P_2\alpha_{s,u}^2 + P_3\alpha_{s,u} + P_4$, where L_{tare} has units of lb and $\alpha_{s,u}$ is in degrees.

$q_u, \mathrm{lb/ft}^2$	P_1	P_2	P_3	P_4
30	1.4620×10^{-2}	3.7414×10^{-2}	1.9260×10^{-1}	1.3281×10^{1}
60	3.2678×10^{-2}	3.2690×10^{-2}	5.6513×10^{-1}	2.7565×10^{1}
90	2.9580×10^{-2}	1.8133×10^{-1}	8.3472×10^{-1}	4.1187×10^{1}

Table A.3: Coefficients for the pitching moment tare polynomials of the form $PM_{tare} = P_1\alpha_{s,u}^2 + P_2\alpha_{s,u} + P_3$, where PM_{tare} has units of $\mathrm{ft\,lb}$ and $\alpha_{s,u}$ is in degrees.

$q_u, \mathrm{lb/ft}^2$	P_1	P_2	P_3
30	-1.0508×10^{-1}	-6.7071×10^{-1}	-5.4343×10^{1}
60	-2.6925×10^{-2}	-1.7007	-1.1615×10^{2}
90	3.7965×10^{-1}	-3.9872	-1.8532×10^{2}

Table A.4: Coefficients for $\alpha_{s,u} = 0$ deg tare polynomials as a function of q_u of the form $X_{tare} = P_1 q_u^2 + P_2 q_u + P_3$, where q_u is in $\mathrm{lb/ft^2}$.

X_{tare}	P_1	P_2	P_3
D_{tare} (lb)	1.5151×10^{-3}	7.1449×10^{-1}	2.7087×10^{-1}
L_{tare} (lb)	—	4.6051×10^{-1}	-2.3538×10^{-1}
PM_{tare} (ft lb)	-4.4310×10^{-3}	-1.6516	-7.8593×10^{-1}

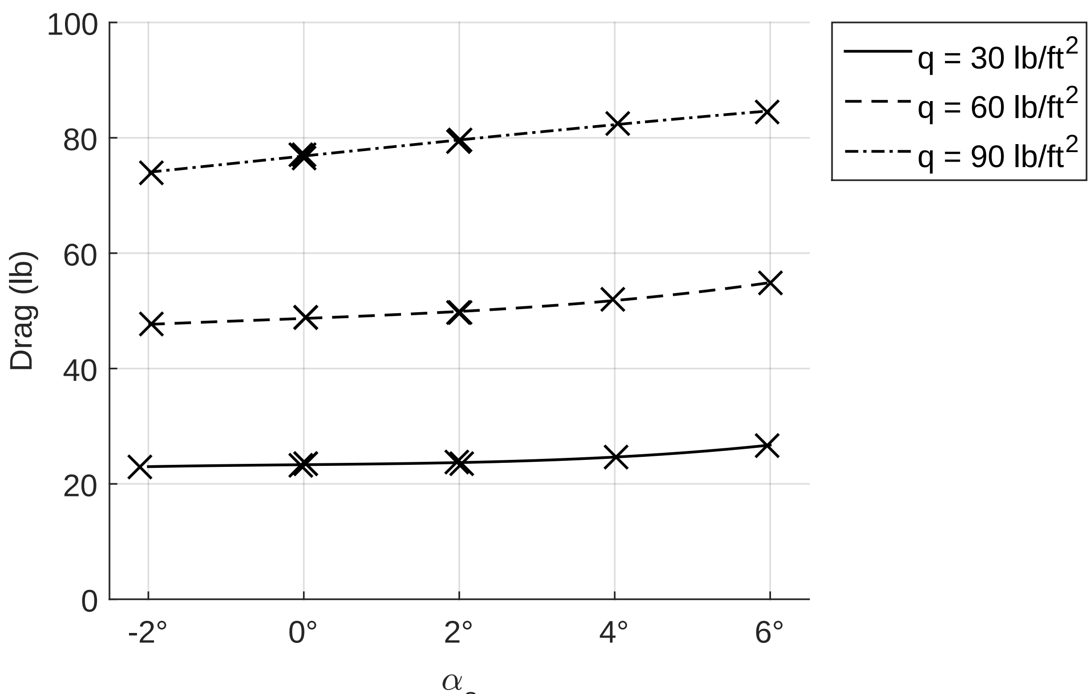

Figure A.1: Aerodynamic tare data and fits for test stand drag

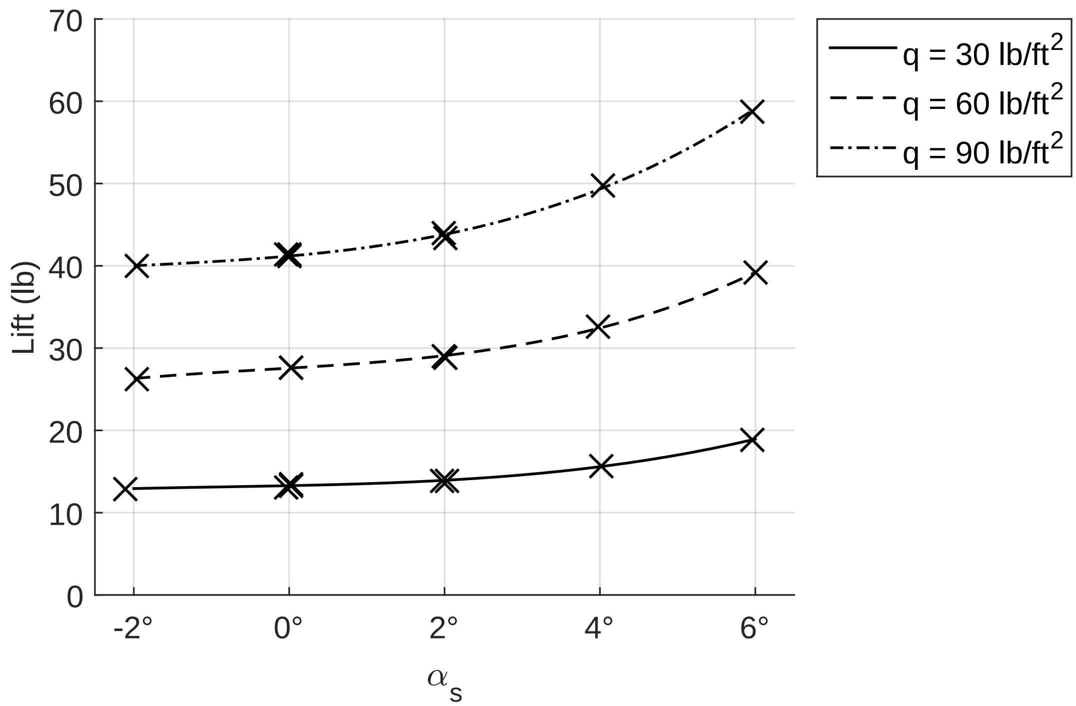

Figure A.2: Aerodynamic tare data and fits for test stand lift

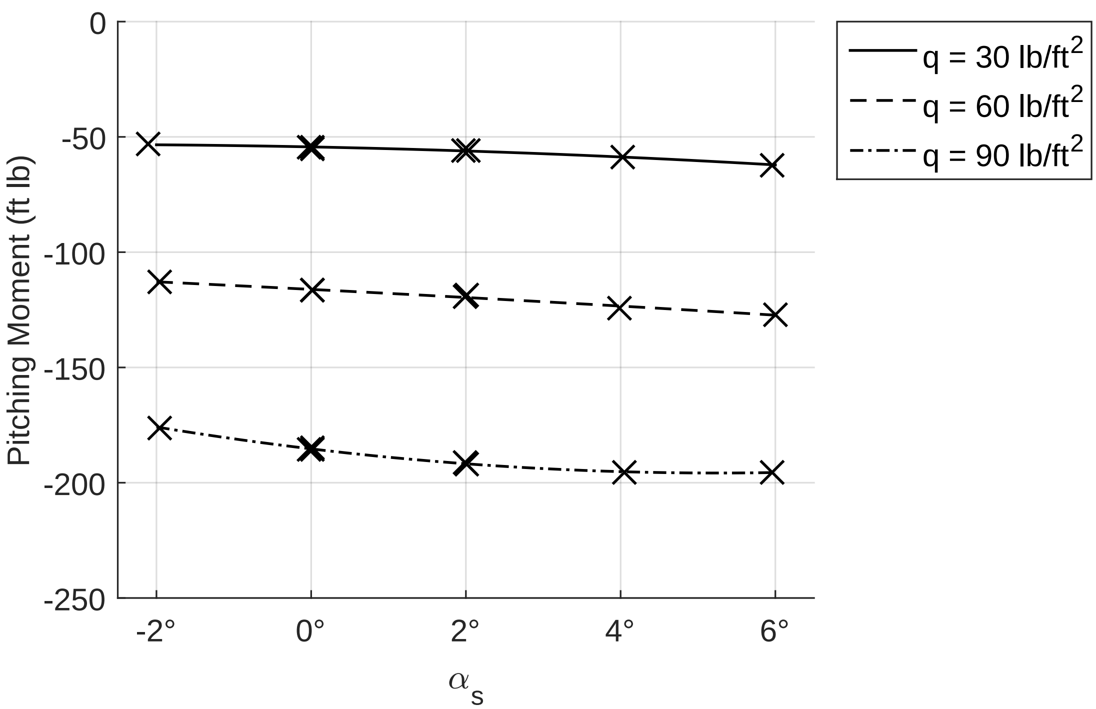

Figure A.3: Aerodynamic tare data and fits for test stand pitching moment

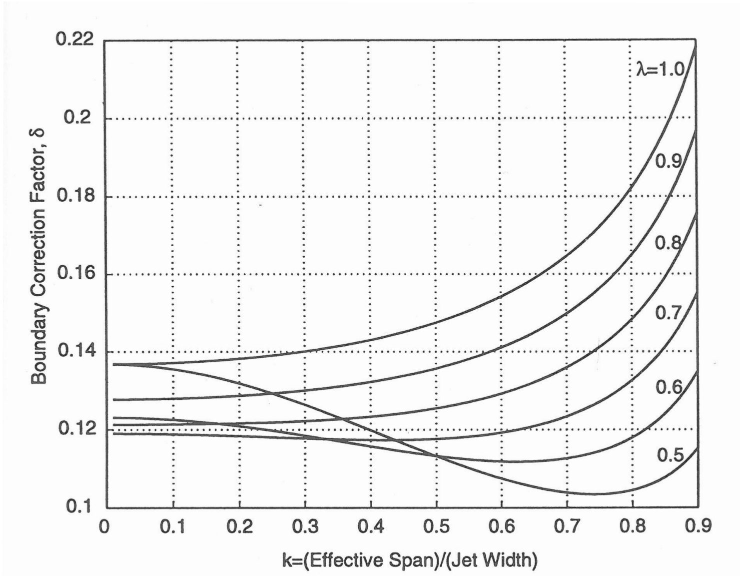

Figure A.4: Boundary correction factor δ for a rectangular closed jet as a function of k, the ratio of model effective span to tunnel jet width, and for various values of λ, the ratio of tunnel height to tunnel width (Barlow, Rae, and Pope 1999).

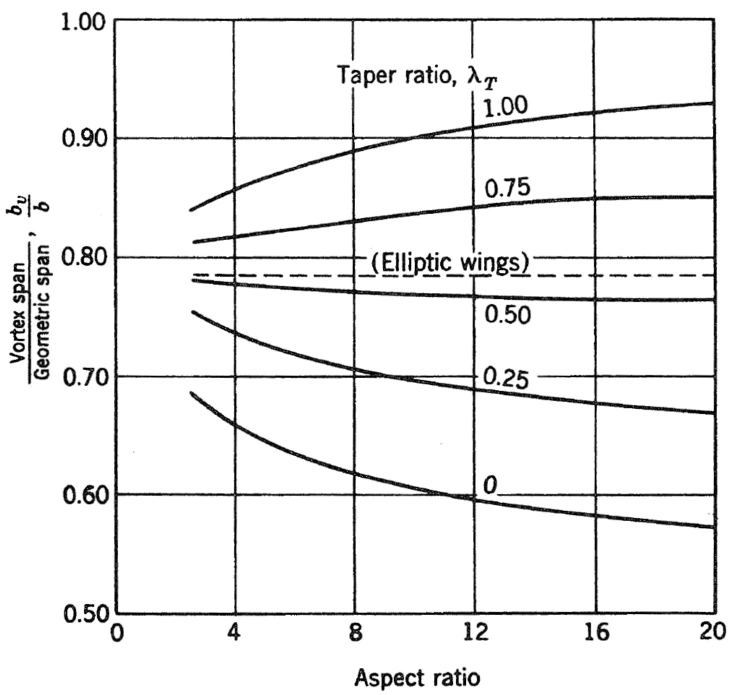

Figure A.5: Vortex span given as a function of taper and aspect ratio, assumed to be $AR = 7.5$ and $\lambda_T = 1$ for this study (Barlow, Rae, and Pope 1999).

Table A.5: Frontal area for each configuration, including test stand, as a function of ψ and α_s.

		S_f for each Configuration including Test Stand, ft^2									
ψ, deg	α_s, deg	0	1	2	3	4	5	6	7	8	9
0.0	−2	1.701	1.825	2.181	2.535	2.887	3.021	3.521	3.211	2.899	2.574
0.0	0	1.695	1.816	2.141	2.450	2.730	2.910	3.385	3.115	2.738	2.458
0.0	2	1.701	1.825	2.183	2.535	2.887	3.021	3.514	3.203	2.898	2.573
0.0	4	1.706	1.833	2.265	2.665	3.077	3.203	3.680	3.312	3.096	2.710
0.0	6	1.709	1.839	2.347	2.783	3.300	3.421	3.840	3.389	3.335	2.840
22.5	−2	–	–	2.192	2.593	2.971	3.067	3.565	3.244	2.978	2.652
22.5	0	–	–	2.111	2.498	2.752	2.919	3.414	3.174	2.752	2.542
22.5	2	–	–	2.193	2.591	2.971	3.067	3.574	3.235	2.985	2.651
22.5	4	–	–	2.295	2.746	3.205	3.309	3.803	3.363	3.230	2.816
22.5	6	–	–	2.391	2.885	3.438	3.558	4.048	3.507	3.474	2.968
45.0	−2	–	–	2.203	2.556	3.001	3.108	3.623	3.182	3.012	2.623
45.0	0	–	–	2.053	2.334	2.576	2.722	3.207	2.973	2.593	2.407
45.0	2	–	–	2.201	2.555	3.001	3.108	3.632	3.187	3.014	2.622
45.0	4	–	–	2.311	2.768	3.293	3.378	3.906	3.388	3.307	2.835
45.0	6	–	–	2.406	2.927	3.530	3.617	4.139	3.543	3.559	3.007
67.5	−2	–	–	2.201	2.564	2.966	3.098	3.598	3.202	2.979	2.606
67.5	0	–	–	2.124	2.437	2.712	2.881	3.285	3.022	2.714	2.440
67.5	2	–	–	2.201	2.562	2.966	3.098	3.591	3.202	2.974	2.605
67.5	4	–	–	2.299	2.742	3.221	3.315	3.836	3.366	3.236	2.800
67.5	6	–	–	2.385	2.880	3.444	3.555	4.045	3.509	3.476	2.951

Table A.6: Frontal area for each configuration, without test stand, as a function of ψ and α_s.

		S_f for each Configuration without Test Stand, ft^2								
ψ, deg	α_s, deg	1	2	3	4	5	6	7	8	9
0.0	−2	0.123	0.480	0.834	1.186	1.319	1.820	1.509	1.197	0.873
0.0	0	0.120	0.445	0.755	1.035	1.214	1.690	1.419	1.042	0.763
0.0	2	0.123	0.482	0.834	1.186	1.319	1.812	1.502	1.197	0.872
0.0	4	0.127	0.559	0.959	1.371	1.497	1.974	1.605	1.390	1.004
0.0	6	0.130	0.638	1.074	1.591	1.712	2.132	1.681	1.626	1.131
22.5	−2	–	0.491	0.892	1.270	1.365	1.863	1.542	1.277	0.950
22.5	0	–	0.416	0.802	1.057	1.224	1.718	1.479	1.057	0.846
22.5	2	–	0.491	0.890	1.270	1.365	1.872	1.534	1.283	0.949
22.5	4	–	0.589	1.040	1.499	1.603	2.097	1.657	1.524	1.110
22.5	6	–	0.682	1.176	1.729	1.849	2.339	1.798	1.765	1.259
45.0	−2	–	0.502	0.854	1.300	1.407	1.921	1.481	1.311	0.921
45.0	0	–	0.358	0.639	0.880	1.026	1.512	1.278	0.897	0.711
45.0	2	–	0.499	0.853	1.300	1.407	1.930	1.486	1.312	0.921
45.0	4	–	0.605	1.062	1.587	1.672	2.200	1.682	1.601	1.129
45.0	6	–	0.697	1.218	1.821	1.908	2.430	1.834	1.851	1.298
67.5	−2	–	0.500	0.863	1.265	1.396	1.897	1.501	1.277	0.905
67.5	0	–	0.429	0.741	1.016	1.186	1.590	1.327	1.018	0.745
67.5	2	–	0.499	0.861	1.265	1.396	1.890	1.500	1.272	0.904
67.5	4	–	0.593	1.036	1.515	1.609	2.130	1.660	1.530	1.094
67.5	6	–	0.676	1.171	1.736	1.847	2.336	1.800	1.768	1.242

Table A.7: Geometric span (perpendicular to the tunnel wall) for each configuration, as a function of ψ. Also given is the vertical projected area of each configuration.

	Model geometric span (b, ft) at				
Configuration	$\psi = 0$ deg	$\psi = 22.5$ deg	$\psi = 45$ deg	$\psi = 67.5$ deg	S_p, ft^2
2	4.185	3.888	3.117	3.940	2.913
3	4.865	4.688	3.890	4.560	4.916
4	6.947	6.648	5.778	6.831	8.817
5	6.947	6.648	5.778	6.831	8.868
6	6.947	6.648	5.778	6.831	9.268
7	4.865	4.688	3.890	4.560	5.369
8	6.947	6.648	5.778	6.831	9.447
9	4.865	4.688	3.890	4.560	5.546
10	6.947	6.648	5.778	6.831	8.817
11	6.947	6.648	5.778	6.831	8.817

Appendix B. Test Article Drawings

Figures B.1, B.3 and B.5 give top and side views of Configurations 4, 6, and 8 respectively. Figures B.2, B.4 and B.6 show a close up of the hub arms of Configurations 4, 6, and 8 respectively, including section cuts at relevant intervals. For a description of each configuration, refer to Table 2.2. Note that Configuration 8 is presented without the covering of aluminum tape to more clearly show the shape and extent of the added fairing.

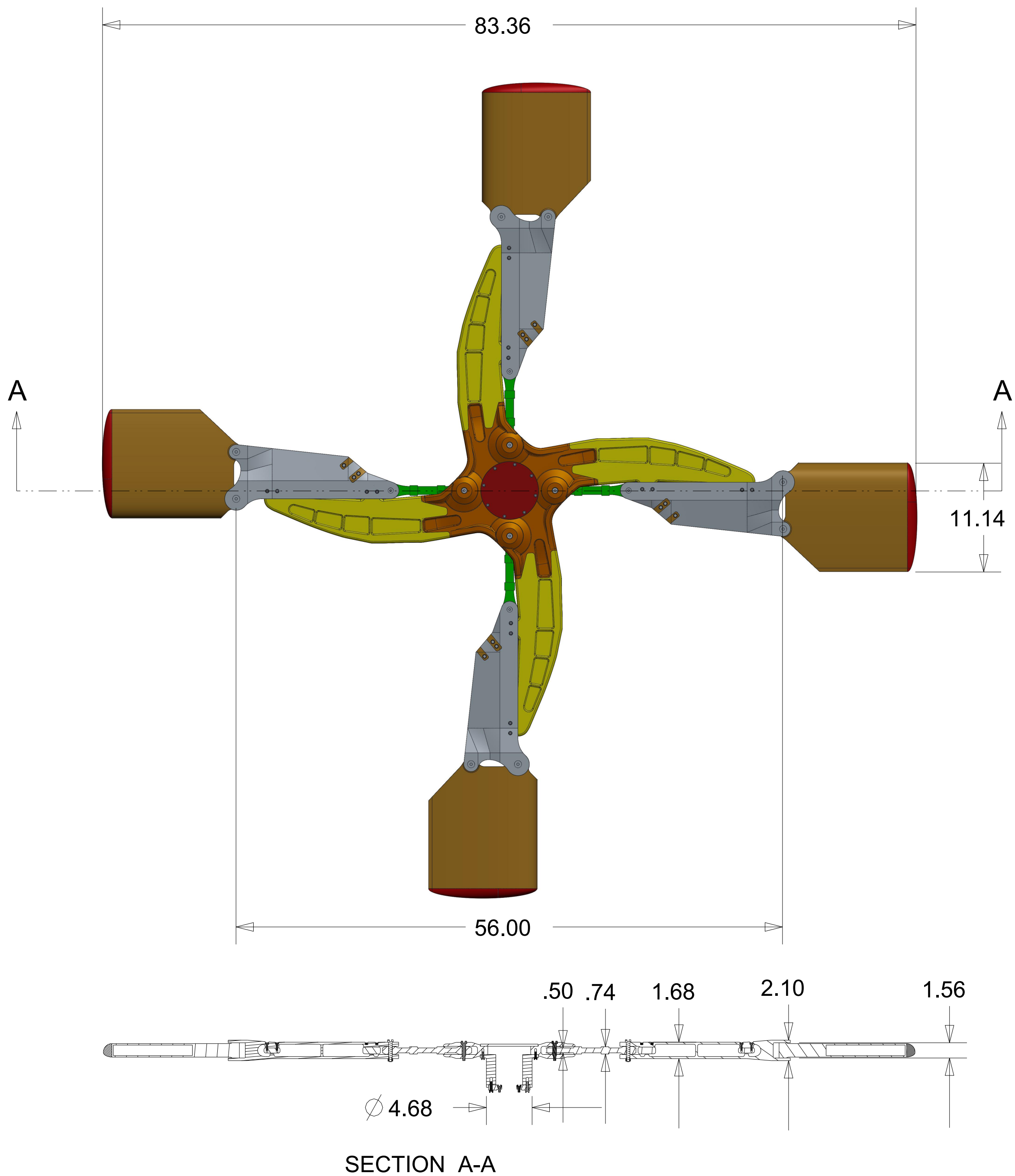

Figure B.1: Top and side view drawings of Configuration 4. Units are inches and degrees.

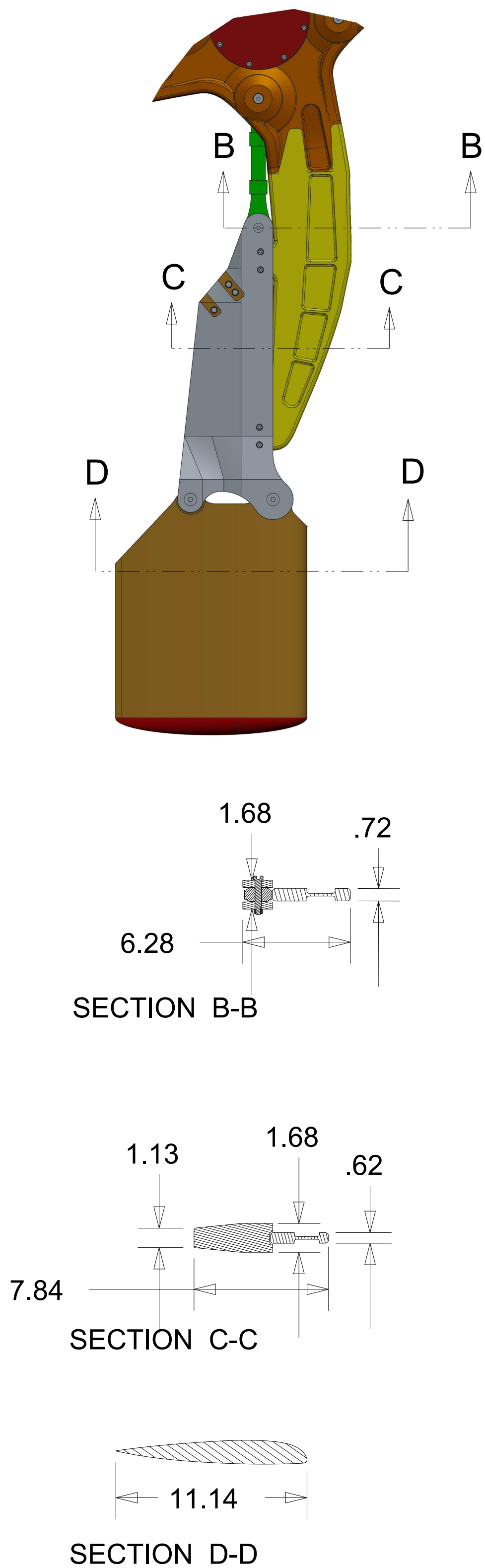

Figure B.2: Inset drawing of the Configuration 4 hub arm. Units are inches and degrees.

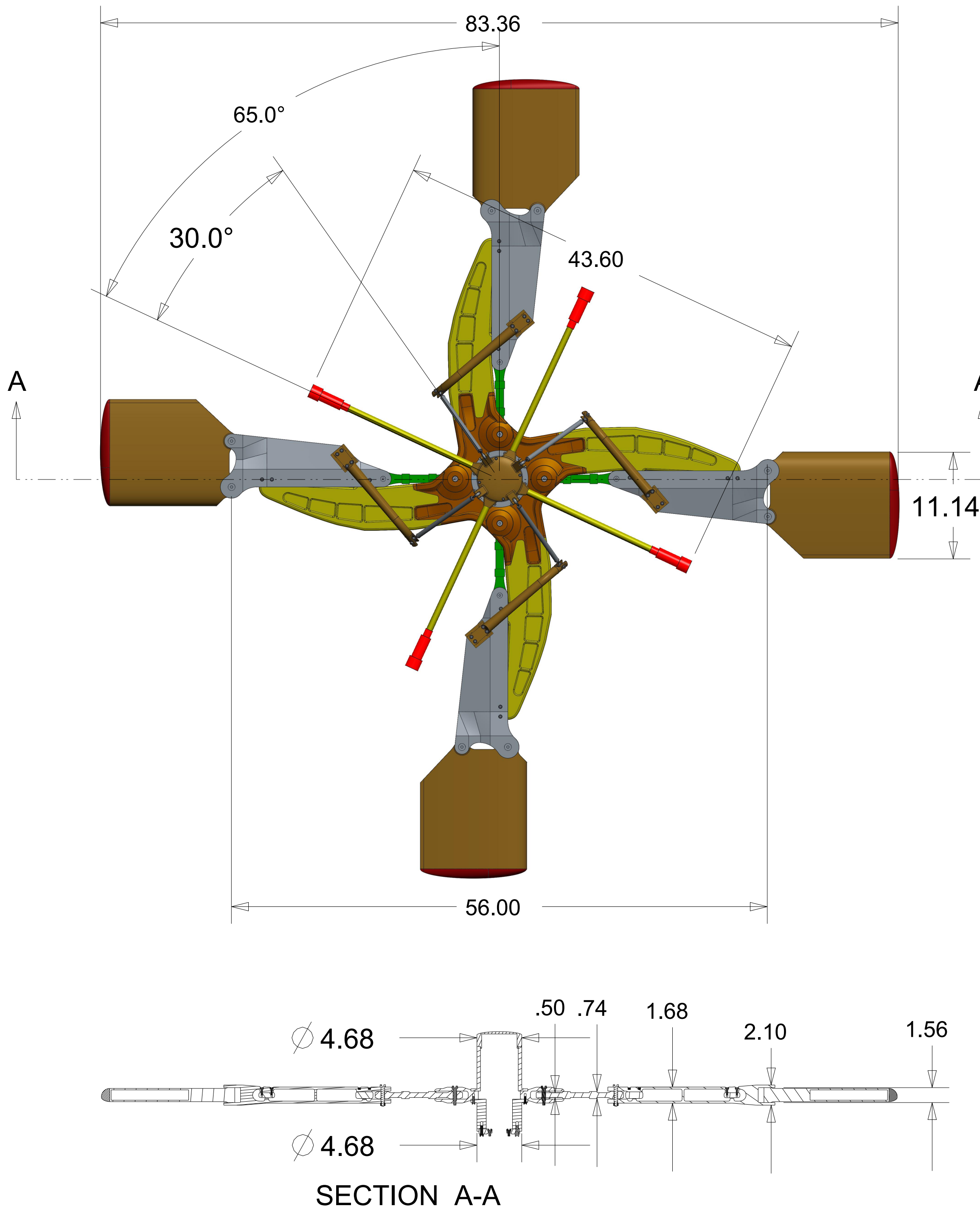

Figure B.3: Top and side views of Configuration 6. Units are inches and degrees.

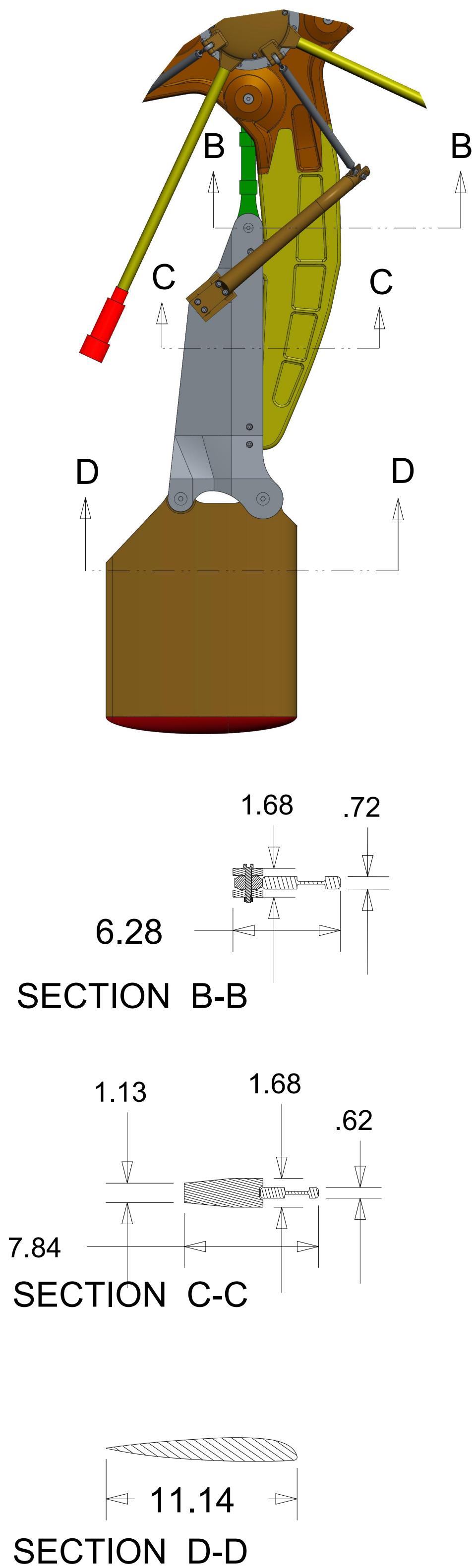

Figure B.4: Inset drawing of the Configuration 6 hub arm. Units are inches and degrees.

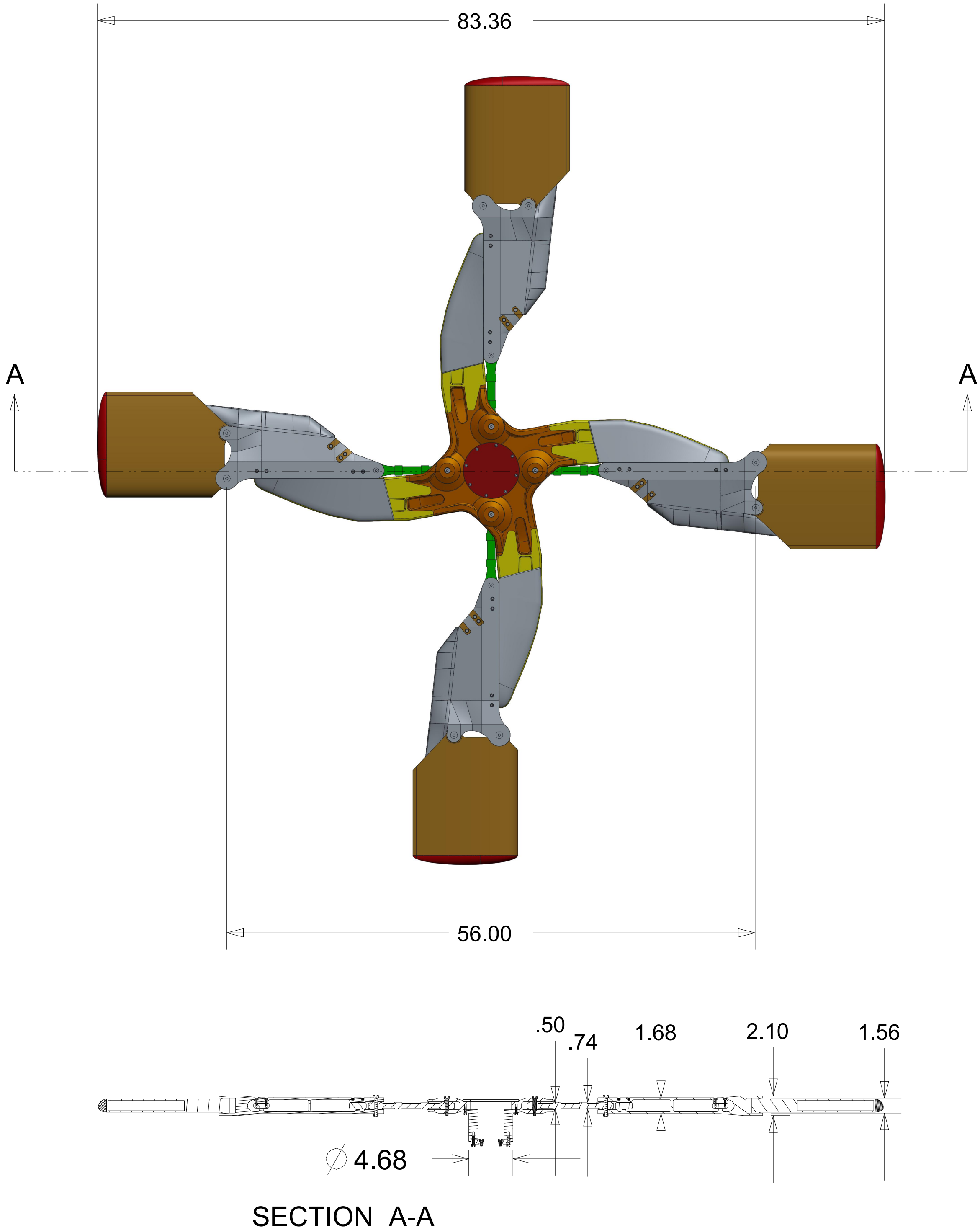

Figure B.5: Top and side section views of Configuration 8. Units are inches and degrees.

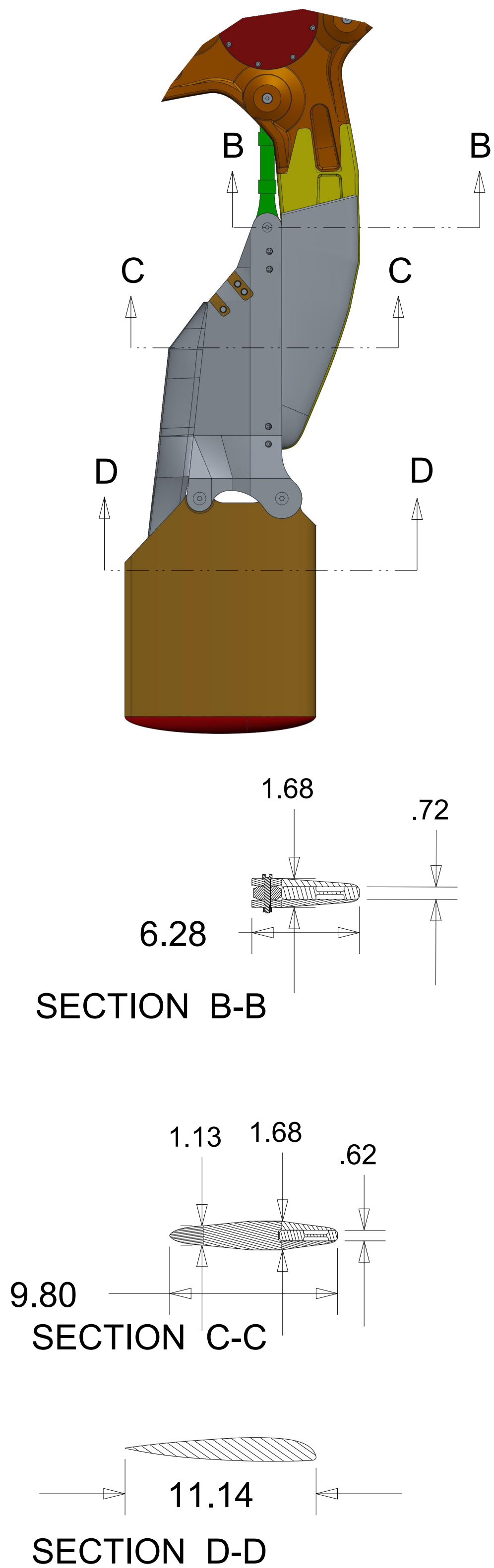

Figure B.6: Inset drawing of the Configuration 8 hub arm. Units are inches and degrees.

Appendix C. Summarized Data

Tables C.1 to C.11 summarize all data collected during this test in both corrected and uncorrected states. The uncorrected data (subscript u) only has weight tares applied, while the corrected data (subscript c) has weight and aerodynamic tares, blockage corrections, and wall corrections applied in that order. Table C.1 give data for the test stand only runs, from which the aerodynamic tares were derived (as described in appendix A). Descriptions of each configuration can be found in Table 2.2.

Table C.1: Summary of data for Configuration 0 (Test Stand Only)

		Tunnel Condition				Force And Moment Data		
Run	$\alpha_{s,u}$ (deg)	q_u (lb/ft^2)	M_u	$Re_u \times 10^6$	v_u (ft/s)	D_u (lb)	L_u (lb)	PM_u (ft lb)
2	0.015	0.00	0.000	0.000	0.0	0.0	0.0	−0.1
2	0.019	30.15	0.143	1.045	157.9	23.4	13.4	−54.8
2	−2.103	30.56	0.144	1.050	159.1	23.0	12.9	−53.0
2	−0.034	30.15	0.143	1.043	158.1	23.2	13.2	−54.4
2	1.959	30.33	0.144	1.045	158.6	23.7	13.9	−55.9
2	4.022	30.34	0.144	1.045	158.6	24.7	15.6	−58.5
2	5.958	30.51	0.144	1.047	159.0	26.7	18.8	−62.3
2	2.040	30.13	0.143	1.040	158.1	23.6	13.9	−55.6
2	0.018	30.17	0.143	1.041	158.2	23.5	13.3	−55.0
2	0.019	60.31	0.204	1.466	225.1	48.8	27.6	−116.4
2	−1.951	60.49	0.205	1.466	225.5	47.6	26.3	−112.6
2	0.024	60.23	0.204	1.462	225.1	48.8	27.6	−116.6
2	2.004	60.50	0.205	1.465	225.6	49.6	28.9	−118.8
2	3.982	60.71	0.205	1.467	226.1	52.0	32.6	−124.1
2	6.001	60.27	0.204	1.461	225.2	54.8	39.2	−127.2
2	1.992	60.44	0.205	1.463	225.6	49.7	29.0	−119.0
2	0.016	60.62	0.205	1.465	226.0	48.8	27.7	−116.8
2	0.014	90.11	0.252	1.780	277.1	77.0	41.3	−185.4
2	−1.958	89.81	0.251	1.773	276.8	74.1	40.0	−176.1
2	−0.029	89.70	0.251	1.771	276.7	76.9	41.4	−185.6
2	1.992	90.41	0.252	1.777	277.9	79.4	43.9	−191.6
2	4.042	90.63	0.252	1.778	278.3	82.4	49.8	−195.3
2	5.962	90.14	0.252	1.773	277.6	84.6	58.8	−195.6
2	2.021	90.42	0.252	1.775	278.1	79.8	43.4	−192.0
2	0.005	90.10	0.252	1.772	277.6	76.6	41.1	−184.9
2	0.001	0.01	0.003	0.023	3.5	0.4	0.2	−1.4

Table C.2: Summary of data for Configuration 1

			Tunnel Condition								Force And Moment Data					
	Model Orientation		Uncorrected				Corrected				Uncorrected			Corrected		
Run	$\alpha_{s,u}$ (deg)	$\alpha_{s,c}$ (deg)	q_u (lb/ft^2)	M_u	$Re_u \times 10^6$	v_u (ft/s)	q_c (lb/ft^2)	M_c	$Re_c \times 10^6$	v_c (ft/s)	D_u (lb)	L_u (lb)	PM_u (ft lb)	D_c (lb)	L_c (lb)	PM_c (ft lb)
3	−0.001	−0.001	0.00	0.001	0.010	1.5	0.00	0.001	0.010	1.5	0.0	0.1	−0.2	−0.2	0.3	0.6
3	0.002	0.002	30.14	0.143	1.035	158.5	30.53	0.144	1.042	159.5	27.1	13.4	−56.4	3.8	0.1	−2.0
3	−1.956	−1.956	30.33	0.144	1.037	159.1	30.73	0.145	1.043	160.1	27.3	12.6	−55.2	4.3	−0.3	−1.8
3	−0.037	−0.037	30.05	0.143	1.031	158.4	30.44	0.144	1.038	159.4	27.6	13.3	−57.2	4.3	0.1	−2.8
3	1.972	1.972	30.10	0.143	1.032	158.5	30.50	0.144	1.038	159.6	27.2	14.4	−56.7	3.5	0.5	−0.6
3	3.950	3.950	30.11	0.143	1.032	158.6	30.50	0.144	1.038	159.6	28.3	16.4	−59.0	3.7	0.9	−0.3
3	5.985	5.985	30.13	0.143	1.032	158.6	30.52	0.144	1.039	159.7	30.2	20.1	−60.9	3.4	1.2	1.2
3	2.038	2.038	30.05	0.143	1.031	158.4	30.45	0.144	1.037	159.5	27.3	14.4	−57.0	3.6	0.5	−0.8
3	0.008	0.008	30.06	0.143	1.031	158.4	30.45	0.144	1.037	159.5	27.6	13.3	−57.3	4.3	0.1	−2.9
3	0.011	0.011	60.15	0.204	1.454	225.4	60.93	0.205	1.463	226.9	55.1	27.5	−117.0	6.5	−0.1	−0.9
3	−1.993	−1.993	60.57	0.205	1.457	226.3	61.36	0.206	1.466	227.8	54.2	26.0	−113.3	6.5	−0.3	−0.4
3	0.038	0.038	60.10	0.204	1.450	225.5	60.89	0.205	1.460	226.9	55.5	27.5	−118.3	6.8	0.0	−2.1
3	1.961	1.961	60.14	0.204	1.451	225.6	60.93	0.205	1.460	227.0	56.0	29.2	−119.8	6.2	0.2	−0.2
3	3.950	3.950	60.29	0.204	1.452	225.9	61.09	0.206	1.462	227.4	57.8	33.8	−123.1	6.0	1.4	0.2
3	5.971	5.971	60.44	0.205	1.454	226.2	61.24	0.206	1.464	227.6	61.0	41.2	−126.4	6.2	2.1	0.9
3	1.985	1.985	60.06	0.204	1.449	225.4	60.84	0.205	1.459	226.9	56.0	29.5	−119.7	6.1	0.4	0.0
3	0.002	0.002	59.88	0.204	1.447	225.1	60.66	0.205	1.456	226.6	55.5	27.3	−118.2	6.9	−0.3	−2.1
3	0.005	0.005	89.76	0.251	1.765	277.3	90.93	0.253	1.776	279.1	85.5	42.1	−185.4	8.6	0.9	−0.1
3	−1.991	−1.991	90.66	0.253	1.772	278.8	91.84	0.254	1.784	280.6	81.6	39.0	−174.0	7.6	−1.0	1.9
3	−0.021	−0.021	89.19	0.250	1.757	276.5	90.35	0.252	1.768	278.3	84.2	38.5	−184.0	7.4	−2.7	1.2
3	1.967	1.967	89.17	0.250	1.756	276.6	90.33	0.252	1.767	278.4	86.2	41.3	−189.8	6.6	−2.5	1.9
3	4.047	4.047	89.00	0.250	1.753	276.4	90.17	0.252	1.765	278.2	90.5	48.3	−197.9	8.2	−1.2	−2.6
3	5.959	5.959	89.71	0.251	1.760	277.5	90.89	0.253	1.772	279.3	91.5	59.0	−194.3	6.9	0.2	1.3
3	2.013	2.013	89.40	0.251	1.756	277.0	90.57	0.252	1.768	278.9	87.1	41.6	−192.4	7.5	−2.3	−0.5
3	0.032	0.032	89.56	0.251	1.758	277.3	90.72	0.253	1.769	279.1	85.0	38.7	−186.1	8.1	−2.5	−0.6
3	0.028	0.028	0.02	0.004	0.026	3.9	0.02	0.004	0.026	4.0	0.5	0.5	−1.6	0.2	0.7	−0.7

Table C.3: Summary of data for Configuration 2

				Tunnel Condition								Force And Moment Data					
	Model Orientation			Uncorrected				Corrected				Uncorrected			Corrected		
Run	ψ (deg)	$\alpha_{s,u}$ (deg)	$\alpha_{s,c}$ (deg)	q_u (lb/ft^2)	M_u	$Re_u \times 10^6$	v_u (ft/s)	q_c (lb/ft^2)	M_c	$Re_c \times 10^6$	v_c (ft/s)	D_u (lb)	L_u (lb)	PM_u (ft lb)	D_c (lb)	L_c (lb)	PM_c (ft lb)
23	0.0	0.007	0.007	0.00	0.001	0.010	1.5	0.00	0.001	0.010	1.5	0.0	0.0	0.1	−0.3	0.3	0.9
23	0.0	0.010	0.039	30.06	0.143	1.003	160.2	30.52	0.144	1.010	161.4	34.5	22.5	−52.1	11.1	9.2	2.3
23	0.0	0.012	0.037	59.82	0.203	1.406	227.6	60.74	0.205	1.417	229.3	70.6	43.0	−110.7	22.0	15.5	5.4
23	0.0	−1.973	−1.981	60.61	0.205	1.413	229.2	61.56	0.206	1.424	231.0	70.6	21.1	−111.3	22.9	−5.3	1.6
23	0.0	−0.019	0.005	60.09	0.204	1.407	228.2	61.01	0.205	1.418	230.0	70.6	42.6	−111.9	22.0	15.0	4.2
23	0.0	1.959	2.011	59.99	0.204	1.406	228.0	60.92	0.205	1.417	229.8	71.9	62.5	−109.8	22.1	33.4	9.8
23	0.0	3.984	4.055	60.35	0.204	1.410	228.7	61.33	0.206	1.422	230.6	75.9	78.1	−110.1	24.2	45.7	13.2
23	0.0	6.005	6.085	60.21	0.204	1.409	228.5	61.23	0.206	1.421	230.4	83.5	89.8	−112.8	28.7	50.6	14.5
23	0.0	1.972	2.025	59.98	0.204	1.406	228.0	60.92	0.205	1.417	229.8	71.8	62.5	−109.4	21.9	33.5	10.2
23	0.0	0.041	0.065	60.31	0.204	1.410	228.6	61.24	0.206	1.421	230.4	70.7	43.3	−111.8	22.0	15.7	4.5
23	0.0	0.033	0.033	0.00	0.000	0.000	0.0	0.00	0.000	0.000	0.0	0.5	0.3	−1.9	0.0	0.5	−1.1
24	22.5	0.032	0.032	0.00	0.001	0.008	1.3	0.00	0.001	0.008	1.3	0.4	0.2	0.8	0.1	0.5	1.5
24	22.5	0.035	0.053	30.25	0.144	1.006	160.7	30.71	0.145	1.014	161.9	34.5	19.2	−49.4	11.1	5.9	5.0
24	22.5	0.038	0.053	60.43	0.205	1.415	228.6	61.35	0.206	1.426	230.3	70.0	37.4	−104.3	21.3	9.8	11.9
24	22.5	−1.950	−1.968	61.50	0.206	1.426	230.8	62.46	0.208	1.437	232.6	70.3	15.1	−106.0	22.7	−11.2	6.9
24	22.5	0.038	0.052	60.00	0.204	1.408	227.9	60.91	0.205	1.418	229.7	69.9	36.8	−104.4	21.2	9.2	11.8
24	22.5	2.004	2.051	60.13	0.204	1.409	228.2	61.08	0.206	1.420	230.0	71.1	58.7	−100.4	21.2	29.6	19.2
24	22.5	3.968	4.041	60.92	0.205	1.418	229.8	61.92	0.207	1.429	231.6	75.0	79.4	−100.1	23.3	47.0	23.3
24	22.5	5.992	6.081	60.80	0.205	1.416	229.5	61.84	0.207	1.428	231.5	82.4	96.7	−104.0	27.7	57.5	23.3
24	22.5	2.020	2.066	60.40	0.205	1.412	228.8	61.35	0.206	1.423	230.6	71.7	58.4	−102.0	21.8	29.3	17.7
24	22.5	0.035	0.050	60.36	0.204	1.411	228.7	61.28	0.206	1.422	230.4	70.3	37.1	−105.3	21.6	9.5	10.9
24	22.5	0.029	0.029	0.01	0.002	0.013	2.1	0.01	0.002	0.013	2.1	0.5	0.3	0.5	0.3	0.5	1.3
25	45.0	0.029	0.029	0.00	0.000	0.000	0.0	0.00	0.000	0.000	0.0	0.4	0.2	0.4	0.0	0.4	1.2
25	45.0	0.030	0.038	30.25	0.144	1.007	160.7	30.70	0.145	1.014	161.9	34.7	16.0	−48.5	11.3	2.7	5.9
25	45.0	0.036	0.041	60.42	0.205	1.416	228.5	61.31	0.206	1.426	230.2	70.4	30.7	−102.9	21.7	3.1	13.3
25	45.0	−1.986	−2.006	61.47	0.206	1.426	230.7	62.44	0.208	1.438	232.5	69.7	13.1	−105.2	22.1	−13.3	7.7
25	45.0	−0.021	−0.017	60.79	0.205	1.418	229.4	61.68	0.207	1.428	231.1	70.3	29.7	−103.4	21.6	2.2	12.7
25	45.0	2.033	2.065	60.17	0.204	1.410	228.2	61.12	0.206	1.422	230.0	71.8	49.2	−99.8	21.9	20.0	19.9
25	45.0	3.962	4.021	60.85	0.205	1.418	229.6	61.86	0.207	1.430	231.5	74.6	69.9	−97.7	22.9	37.6	25.6
25	45.0	6.027	6.116	60.99	0.206	1.420	229.8	62.05	0.207	1.432	231.8	81.9	96.5	−99.5	27.1	57.2	27.8
25	45.0	1.965	1.996	60.26	0.204	1.412	228.4	61.21	0.206	1.423	230.2	71.1	48.9	−98.9	21.3	19.9	20.7
25	45.0	0.038	0.043	60.26	0.204	1.412	228.4	61.15	0.206	1.422	230.1	70.3	30.8	−103.1	21.6	3.2	13.1
25	45.0	0.031	0.031	0.01	0.002	0.016	2.5	0.01	0.002	0.016	2.5	0.5	0.3	0.6	0.2	0.5	1.4
26	67.5	0.031	0.031	0.00	0.001	0.008	1.3	0.00	0.001	0.008	1.3	0.2	0.2	1.5	−0.1	0.5	2.3
26	67.5	0.033	0.051	30.17	0.143	1.007	160.3	30.63	0.145	1.015	161.6	35.0	19.0	−48.9	11.7	5.8	5.4
26	67.5	0.037	0.051	60.01	0.204	1.415	227.5	60.92	0.205	1.425	229.3	70.7	36.7	−107.0	22.0	9.1	9.2
26	67.5	−2.018	−2.034	61.07	0.206	1.424	229.8	62.03	0.207	1.436	231.6	70.6	16.0	−107.5	23.0	−10.3	5.3
26	67.5	−0.022	−0.010	60.01	0.204	1.412	227.7	60.93	0.205	1.422	229.5	70.9	35.5	−108.1	22.3	7.9	8.0
26	67.5	2.035	2.079	60.47	0.205	1.417	228.6	61.42	0.206	1.428	230.4	72.8	56.8	−106.4	23.0	27.7	13.3
26	67.5	3.964	4.033	61.03	0.206	1.423	229.7	62.04	0.207	1.435	231.6	76.6	77.1	−106.2	24.9	44.7	17.2
26	67.5	5.983	6.070	60.91	0.205	1.422	229.5	61.95	0.207	1.434	231.4	84.9	95.1	−107.6	30.1	56.0	19.6
26	67.5	2.014	2.057	60.45	0.205	1.417	228.6	61.40	0.206	1.428	230.4	72.6	56.3	−105.9	22.7	27.2	13.8
26	67.5	−0.006	0.007	60.47	0.205	1.417	228.6	61.39	0.206	1.428	230.4	70.8	36.1	−107.6	22.1	8.5	8.5
26	67.5	−0.013	−0.013	0.01	0.003	0.020	3.1	0.01	0.003	0.020	3.1	0.6	0.3	0.2	0.3	0.5	1.0

Table C.4: Summary of data for Configuration 3

				Tunnel Condition								Force And Moment Data					
	Model Orientation			Uncorrected				Corrected				Uncorrected			Corrected		
Run	ψ (deg)	$\alpha_{s,u}$ (deg)	$\alpha_{s,c}$ (deg)	q_u (lb/ft^2)	M_u	$Re_u \times 10^6$	v_u (ft/s)	q_c (lb/ft^2)	M_c	$Re_c \times 10^6$	v_c (ft/s)	D_u (lb)	L_u (lb)	PM_u (ft lb)	D_c (lb)	L_c (lb)	PM_c (ft lb)
22	0.0	−0.051	−0.051	0.00	0.000	0.000	0.0	0.00	0.000	0.000	0.0	0.1	−0.1	−3.3	0.0	0.1	−2.5
22	0.0	−0.048	−0.028	30.17	0.143	0.999	160.8	30.70	0.145	1.008	162.3	42.9	19.7	−53.4	19.6	6.4	0.9
22	0.0	−0.041	−0.024	60.19	0.204	1.405	228.6	61.25	0.206	1.417	230.6	87.5	38.3	−111.7	38.9	10.8	4.4
22	0.0	−2.007	−2.025	60.95	0.205	1.412	230.2	62.06	0.207	1.425	232.3	87.1	14.8	−112.9	39.5	−11.5	0.0
22	0.0	0.008	0.026	60.28	0.204	1.404	228.9	61.34	0.206	1.417	230.9	87.5	39.0	−111.5	38.8	11.4	4.6
22	0.0	2.011	2.059	60.10	0.204	1.402	228.6	61.19	0.206	1.414	230.7	91.1	59.5	−107.0	41.3	30.4	12.7
22	0.0	4.003	4.076	60.12	0.204	1.402	228.7	61.27	0.206	1.415	230.8	96.6	78.9	−104.3	44.9	46.5	19.1
22	0.0	6.009	6.095	59.67	0.203	1.396	227.8	60.86	0.205	1.410	230.1	105.8	93.2	−104.1	51.0	54.0	23.2
22	0.0	1.974	2.021	60.45	0.205	1.405	229.3	61.55	0.206	1.418	231.4	91.0	59.3	−106.9	41.1	30.3	12.7
22	0.0	−0.008	0.010	60.13	0.204	1.402	228.7	61.19	0.206	1.414	230.7	87.7	39.1	−111.8	39.0	11.5	4.3
22	0.0	−0.012	−0.012	0.01	0.002	0.013	2.1	0.01	0.002	0.013	2.2	0.0	−0.2	−2.3	−0.2	0.0	−1.5
21	22.5	0.033	0.033	0.00	0.001	0.008	1.3	0.00	0.001	0.008	1.3	−0.1	−0.1	−0.3	−0.3	0.1	0.5
21	22.5	0.036	0.057	30.12	0.143	1.001	160.5	30.66	0.145	1.010	161.9	41.8	19.7	−49.9	18.5	6.4	4.4
21	22.5	0.042	0.057	60.29	0.204	1.407	228.7	61.37	0.206	1.420	230.7	85.8	37.3	−105.3	37.1	9.7	10.9
21	22.5	−1.978	−2.001	60.90	0.205	1.413	229.9	62.03	0.207	1.426	232.1	85.7	11.1	−107.3	38.0	−15.2	5.6
21	22.5	0.035	0.049	60.18	0.204	1.405	228.6	61.26	0.206	1.417	230.6	85.8	37.0	−106.2	37.1	9.4	10.0
21	22.5	2.003	2.054	60.20	0.204	1.405	228.6	61.32	0.206	1.418	230.7	88.5	61.8	−101.6	38.6	32.7	18.1
21	22.5	4.043	4.121	60.23	0.204	1.405	228.7	61.42	0.206	1.419	230.9	95.0	82.2	−98.3	43.3	49.7	25.1
21	22.5	6.016	6.117	59.84	0.203	1.400	227.9	61.08	0.206	1.415	230.3	103.9	103.4	−96.2	49.1	64.1	31.2
21	22.5	2.021	2.072	59.57	0.203	1.397	227.4	60.67	0.205	1.410	229.5	88.7	61.7	−102.7	38.8	32.6	17.0
21	22.5	−0.043	−0.030	60.19	0.204	1.404	228.7	61.27	0.206	1.416	230.7	85.8	35.9	−106.1	37.1	8.3	10.0
21	22.5	−0.051	−0.051	0.01	0.003	0.019	3.1	0.01	0.003	0.020	3.1	0.6	0.1	−2.6	0.3	0.4	−1.8
20	45.0	−0.052	−0.052	0.01	0.002	0.015	2.4	0.01	0.002	0.015	2.4	0.5	−0.1	−4.5	0.2	0.1	−3.7
20	45.0	−0.045	−0.037	30.03	0.143	1.007	159.8	30.54	0.144	1.016	161.1	41.5	15.5	−51.0	18.2	2.3	3.3
20	45.0	−0.041	−0.037	60.31	0.204	1.415	228.3	61.32	0.206	1.427	230.2	84.6	30.2	−103.7	36.0	2.7	12.3
20	45.0	−2.026	−2.058	61.06	0.206	1.422	229.8	62.19	0.207	1.435	231.9	84.6	5.7	−107.9	37.0	−20.5	4.9
20	45.0	−0.024	−0.019	60.26	0.204	1.412	228.3	61.27	0.206	1.424	230.2	84.4	30.5	−103.6	35.8	3.0	12.5
20	45.0	2.029	2.073	60.29	0.204	1.411	228.4	61.40	0.206	1.424	230.5	86.6	57.1	−95.7	36.7	28.0	24.0
20	45.0	4.018	4.100	60.22	0.204	1.410	228.3	61.41	0.206	1.424	230.6	92.1	84.6	−91.4	40.4	52.1	32.0
20	45.0	6.040	6.161	59.99	0.204	1.407	228.0	61.26	0.206	1.421	230.3	101.4	116.6	−86.2	46.6	77.2	41.2
20	45.0	1.990	2.033	60.16	0.204	1.408	228.3	61.27	0.206	1.420	230.4	86.3	56.4	−95.5	36.4	27.3	24.1
20	45.0	0.043	0.050	59.92	0.204	1.404	227.9	60.92	0.205	1.416	229.8	84.5	31.6	−103.7	35.8	4.0	12.5
20	45.0	0.034	0.034	0.02	0.003	0.023	3.7	0.02	0.003	0.023	3.7	0.6	0.2	−4.8	0.3	0.4	−4.0
19	67.5	0.025	0.025	0.01	0.002	0.015	2.2	0.01	0.002	0.015	2.3	0.0	0.0	0.0	−0.3	0.2	0.8
19	67.5	0.030	0.041	30.13	0.143	1.023	159.0	30.66	0.144	1.032	160.4	41.7	17.1	−47.9	18.4	3.8	6.4
19	67.5	0.033	0.042	59.97	0.203	1.431	226.1	61.02	0.205	1.443	228.1	84.3	33.3	−102.5	35.6	5.8	13.7
19	67.5	−2.003	−2.029	60.89	0.205	1.438	228.1	62.01	0.207	1.452	230.2	84.9	9.4	−107.9	37.2	−16.9	5.0
19	67.5	−0.017	−0.008	60.10	0.204	1.428	226.6	61.15	0.205	1.440	228.6	84.7	33.0	−103.6	36.0	5.4	12.5
19	67.5	2.010	2.056	59.95	0.203	1.426	226.4	61.05	0.205	1.439	228.5	86.5	58.7	−97.5	36.7	29.6	22.2
19	67.5	3.959	4.042	59.69	0.203	1.422	225.9	60.87	0.205	1.436	228.1	92.6	85.0	−95.3	40.9	52.6	28.0
19	67.5	6.033	6.152	59.54	0.203	1.420	225.6	60.77	0.205	1.435	228.0	102.5	114.5	−92.1	47.7	75.2	35.3
19	67.5	2.039	2.086	59.71	0.203	1.421	226.0	60.81	0.205	1.434	228.1	86.8	59.0	−97.4	36.9	29.9	22.4
19	67.5	−0.041	−0.032	59.68	0.203	1.421	226.0	60.72	0.205	1.433	228.0	84.4	32.8	−103.5	35.7	5.3	12.6
19	67.5	−0.049	−0.049	0.00	0.000	0.000	0.0	0.00	0.000	0.000	0.0	0.2	0.0	−0.4	0.0	0.2	0.4

Table C.5: Summary of data for Configuration 4

	Model Orientation			Tunnel Condition								Force And Moment Data					
				Uncorrected				Corrected				Uncorrected			Corrected		
Run	ψ (deg)	$\alpha_{s,u}$ (deg)	$\alpha_{s,c}$ (deg)	q_u (lb/ft^2)	M_u	$Re_u \times 10^6$	v_u (ft/s)	q_c (lb/ft^2)	M_c	$Re_c \times 10^6$	v_c (ft/s)	D_u (lb)	L_u (lb)	PM_u (ft lb)	D_c (lb)	L_c (lb)	PM_c (ft lb)
15	0.0	0.021	0.021	0.00	0.001	0.011	1.7	0.00	0.002	0.011	1.7	0.0	0.0	0.0	−0.3	0.2	0.8
15	0.0	0.028	0.066	29.88	0.142	1.037	157.2	30.46	0.144	1.047	158.7	44.4	24.9	−48.8	21.1	11.7	5.5
15	0.0	0.028	0.064	59.95	0.203	1.459	224.3	61.13	0.205	1.474	226.4	91.4	49.7	−104.8	42.7	22.1	11.4
15	0.0	−1.981	−1.998	60.36	0.204	1.462	225.2	61.61	0.206	1.477	227.5	91.3	16.0	−115.3	43.6	−10.3	−2.5
15	0.0	0.025	0.061	59.91	0.203	1.455	224.4	61.08	0.205	1.470	226.6	91.2	49.6	−104.4	42.5	22.0	11.8
15	0.0	1.992	2.073	60.11	0.204	1.457	224.8	61.36	0.206	1.472	227.1	96.2	79.1	−94.5	46.4	50.0	25.2
15	0.0	4.024	4.146	60.32	0.204	1.459	225.2	61.66	0.206	1.475	227.7	105.2	108.3	−88.0	53.5	75.9	35.4
15	0.0	6.010	6.169	60.35	0.204	1.459	225.3	61.78	0.206	1.476	228.0	116.4	138.3	−80.9	61.8	99.1	46.5
15	0.0	2.036	2.119	60.13	0.204	1.456	224.9	61.37	0.206	1.471	227.2	96.4	80.0	−94.2	46.5	50.9	25.5
15	0.0	−0.020	0.015	60.36	0.204	1.458	225.4	61.54	0.206	1.473	227.6	91.8	49.4	−105.7	43.1	21.8	10.4
15	0.0	−0.025	−0.025	0.00	0.002	0.012	1.8	0.00	0.002	0.012	1.8	0.5	0.1	−1.5	0.2	0.3	−0.7
16	22.5	−0.027	−0.027	0.00	0.001	0.005	0.7	0.00	0.001	0.005	0.7	0.1	−0.1	−1.8	−0.2	0.1	−1.0
16	22.5	−0.021	0.005	30.13	0.143	1.036	158.2	30.73	0.144	1.046	159.7	43.8	21.6	−47.8	20.5	8.3	6.5
16	22.5	−0.020	0.001	59.77	0.203	1.449	224.4	60.95	0.205	1.463	226.6	88.8	41.0	−95.4	40.1	13.5	20.7
16	22.5	−2.037	−2.086	60.83	0.205	1.461	226.5	62.13	0.207	1.477	228.9	90.4	−4.9	−106.6	42.8	−31.2	6.2
16	22.5	0.030	0.053	60.04	0.203	1.450	225.0	61.23	0.205	1.465	227.2	89.4	42.0	−96.2	40.7	14.4	20.0
16	22.5	2.005	2.093	60.55	0.204	1.456	226.0	61.85	0.206	1.471	228.4	92.9	84.5	−81.9	43.1	55.4	37.8
16	22.5	3.969	4.120	60.57	0.204	1.455	226.1	61.96	0.207	1.472	228.7	100.9	127.6	−72.9	49.4	95.2	50.4
16	22.5	5.983	6.195	60.20	0.204	1.450	225.4	61.69	0.206	1.468	228.2	113.9	172.6	−63.6	59.6	133.5	63.7
16	22.5	1.968	2.056	60.18	0.204	1.450	225.4	61.47	0.206	1.465	227.8	92.9	84.1	−82.0	43.1	55.0	37.6
16	22.5	0.013	0.035	59.91	0.203	1.446	224.9	61.09	0.205	1.460	227.1	89.0	41.6	−96.4	40.3	14.0	19.8
16	22.5	0.003	0.003	0.01	0.003	0.022	3.4	0.01	0.003	0.022	3.4	0.6	0.0	−3.4	0.3	0.2	−2.6
17	45.0	0.002	0.002	0.00	0.000	0.000	0.0	0.00	0.000	0.000	0.0	0.1	−0.1	−1.1	0.0	0.2	−0.3
17	45.0	0.006	0.028	30.30	0.143	1.035	158.8	30.86	0.145	1.044	160.3	43.7	20.4	−42.9	20.3	7.1	11.4
17	45.0	0.012	0.030	59.98	0.203	1.448	225.0	61.09	0.205	1.461	227.1	88.4	39.3	−89.3	39.7	11.7	26.9
17	45.0	−2.026	−2.079	60.44	0.204	1.451	226.0	61.75	0.206	1.466	228.5	88.7	−7.9	−106.1	41.1	−34.2	6.8
17	45.0	0.020	0.039	59.81	0.203	1.441	224.9	60.91	0.205	1.455	227.0	88.2	39.7	−88.6	39.5	12.2	27.6
17	45.0	2.038	2.132	60.42	0.204	1.448	226.1	61.73	0.206	1.464	228.6	92.4	88.9	−67.2	42.6	59.8	52.6
17	45.0	3.965	4.133	60.68	0.204	1.451	226.7	62.12	0.207	1.468	229.3	100.0	139.9	−47.2	48.5	107.5	76.2
17	45.0	5.976	6.216	60.34	0.204	1.446	226.1	61.87	0.206	1.465	228.9	112.9	192.7	−28.7	58.7	153.6	98.5
17	45.0	2.008	2.101	60.39	0.204	1.446	226.2	61.69	0.206	1.462	228.6	92.2	88.7	−67.3	42.4	59.6	52.3
17	45.0	−0.027	−0.009	59.74	0.203	1.439	224.9	60.85	0.205	1.452	227.0	88.1	39.0	−88.5	39.4	11.5	27.6
17	45.0	−0.031	−0.031	0.01	0.002	0.015	2.4	0.01	0.002	0.015	2.4	0.5	0.1	−2.9	0.3	0.3	−2.1
18	67.5	−0.032	−0.032	0.01	0.002	0.014	2.1	0.01	0.002	0.014	2.1	0.2	0.0	−2.8	−0.1	0.2	−2.0
18	67.5	−0.028	0.007	19.79	0.116	0.833	128.4	20.18	0.117	0.841	129.6	29.0	16.1	−28.5	14.0	7.2	6.8
18	67.5	−0.026	0.009	29.81	0.142	1.020	157.9	30.39	0.144	1.030	159.5	43.7	24.1	−42.9	20.3	10.8	11.4
18	67.5	−1.976	−2.009	30.26	0.143	1.027	159.2	30.90	0.145	1.038	160.9	44.7	2.6	−54.6	21.7	−10.4	−1.2
18	67.5	−0.051	−0.018	29.83	0.142	1.019	158.1	30.42	0.144	1.029	159.6	43.7	23.6	−43.5	20.3	10.3	10.8
18	67.5	2.003	2.109	29.92	0.142	1.021	158.3	30.55	0.144	1.031	160.0	46.1	46.7	−33.7	22.5	32.8	22.4
18	67.5	4.021	4.198	29.85	0.142	1.019	158.2	30.55	0.144	1.031	160.0	50.7	70.5	−26.5	26.2	54.9	32.3
18	67.5	6.046	6.292	29.75	0.142	1.017	157.9	30.48	0.144	1.030	159.8	57.1	94.8	−23.2	30.6	75.8	39.1
18	67.5	1.966	2.074	29.93	0.143	1.020	158.4	30.56	0.144	1.031	160.0	46.3	47.1	−33.3	22.7	33.2	22.7
18	67.5	−0.024	0.011	29.83	0.142	1.018	158.1	30.41	0.144	1.028	159.6	44.1	24.3	−44.1	20.8	11.0	10.3
18	67.5	−0.029	0.003	40.26	0.166	1.181	184.1	41.04	0.167	1.193	185.9	59.2	31.8	−59.8	27.7	13.5	14.7
18	67.5	−0.031	0.000	50.47	0.186	1.321	206.6	51.46	0.188	1.333	208.6	74.4	39.0	−75.9	34.2	16.0	19.5
18	67.5	−0.026	0.003	59.79	0.203	1.434	225.3	60.95	0.205	1.448	227.5	87.7	45.4	−89.9	39.0	17.8	26.2
18	67.5	−2.026	−2.064	60.48	0.204	1.441	226.7	61.77	0.206	1.457	229.2	88.9	2.6	−112.4	41.3	−23.7	0.4
18	67.5	0.043	0.073	59.62	0.203	1.430	225.1	60.78	0.205	1.444	227.3	87.6	46.4	−89.2	38.9	18.8	27.0
18	67.5	1.958	2.056	60.04	0.203	1.435	226.0	61.31	0.206	1.450	228.4	92.0	90.2	−69.4	42.2	61.2	50.2
18	67.5	4.002	4.173	59.45	0.202	1.427	224.9	60.82	0.205	1.444	227.5	100.9	137.6	−52.4	49.4	105.2	71.0
18	67.5	6.021	6.260	59.29	0.202	1.425	224.6	60.76	0.205	1.442	227.4	113.8	186.1	−40.3	59.5	146.8	87.1
18	67.5	2.031	2.133	59.53	0.203	1.427	225.1	60.79	0.205	1.442	227.5	92.3	92.3	−68.4	42.5	63.2	51.3
18	67.5	0.027	0.058	59.48	0.202	1.426	225.0	60.64	0.204	1.440	227.2	88.2	46.5	−90.7	39.5	19.0	25.5
18	67.5	0.017	0.017	0.02	0.004	0.029	4.5	0.03	0.004	0.030	4.6	0.6	0.0	−4.0	0.3	0.3	−3.2

Table C.6: Summary of data for Configuration 5

				Tunnel Condition								Force And Moment Data					
	Model Orientation			Uncorrected				Corrected				Uncorrected			Corrected		
Run	ψ (deg)	$\alpha_{s,u}$ (deg)	$\alpha_{s,c}$ (deg)	q_u (lb/ft^2)	M_u	$Re_u \times 10^6$	v_u (ft/s)	q_c (lb/ft^2)	M_c	$Re_c \times 10^6$	v_c (ft/s)	D_u (lb)	L_u (lb)	PM_u (ft lb)	D_c (lb)	L_c (lb)	PM_c (ft lb)
14	0.0	0.012	0.012	0.00	0.000	0.000	0.0	0.00	0.000	0.000	0.0	0.3	0.3	−1.7	0.0	0.5	−0.9
14	0.0	0.017	0.037	29.84	0.142	1.037	157.1	30.46	0.144	1.048	158.7	49.2	19.5	−51.9	25.8	6.2	2.4
14	0.0	0.022	0.040	60.55	0.204	1.473	225.1	61.82	0.207	1.488	227.4	100.4	38.4	−109.9	51.7	10.8	6.3
14	0.0	−2.044	−2.076	60.36	0.204	1.468	224.8	61.67	0.206	1.484	227.3	101.6	6.2	−117.1	54.0	−20.1	−4.3
14	0.0	−0.008	0.009	59.99	0.203	1.462	224.2	61.25	0.206	1.478	226.5	100.3	38.0	−110.2	51.6	10.5	6.0
14	0.0	2.013	2.081	60.06	0.204	1.463	224.4	61.36	0.206	1.479	226.8	104.0	71.2	−99.8	54.1	42.1	19.9
14	0.0	3.954	4.064	60.30	0.204	1.465	224.8	61.68	0.206	1.482	227.4	111.0	100.3	−92.9	59.4	68.0	30.4
14	0.0	5.986	6.140	60.25	0.204	1.464	224.8	61.73	0.206	1.482	227.5	123.0	135.4	−84.8	68.4	96.2	42.5
14	0.0	1.967	2.035	60.12	0.204	1.463	224.5	61.42	0.206	1.478	227.0	104.0	71.1	−100.0	54.1	42.0	19.6
14	0.0	−0.038	−0.022	59.97	0.203	1.460	224.3	61.22	0.205	1.476	226.6	100.4	37.4	−110.1	51.7	9.9	5.9
14	0.0	−0.047	−0.047	0.01	0.002	0.016	2.3	0.01	0.002	0.016	2.4	0.6	0.5	−2.6	0.3	0.7	−1.8
13	22.5	−0.048	−0.048	0.01	0.002	0.018	2.7	0.01	0.002	0.018	2.7	0.1	0.0	−2.2	−0.2	0.2	−1.4
13	22.5	−0.041	−0.038	30.20	0.143	1.045	157.9	30.83	0.145	1.056	159.6	49.1	14.3	−56.2	25.8	1.1	−1.9
13	22.5	−0.036	−0.038	60.24	0.204	1.471	224.4	61.50	0.206	1.487	226.7	99.5	26.8	−114.6	50.8	−0.8	1.5
13	22.5	−2.022	−2.092	60.92	0.205	1.477	225.8	62.26	0.207	1.493	228.3	100.9	−18.3	−124.7	53.3	−44.6	−11.9
13	22.5	−0.034	−0.035	60.06	0.204	1.465	224.2	61.32	0.206	1.481	226.6	99.0	27.0	−114.4	50.4	−0.6	1.7
13	22.5	1.970	2.034	60.28	0.204	1.467	224.7	61.60	0.206	1.483	227.1	101.6	69.7	−98.4	51.8	40.6	21.2
13	22.5	3.974	4.100	60.36	0.204	1.468	224.9	61.80	0.207	1.485	227.5	109.3	111.3	−82.4	57.8	78.9	41.0
13	22.5	5.990	6.174	60.78	0.205	1.472	225.7	62.34	0.207	1.491	228.6	121.7	155.5	−69.1	67.2	116.3	58.2
13	22.5	2.030	2.098	60.18	0.204	1.465	224.6	61.51	0.206	1.481	227.0	101.9	71.3	−97.6	52.0	42.2	22.1
13	22.5	0.026	0.028	59.76	0.203	1.460	223.8	61.01	0.205	1.475	226.1	99.3	29.0	−114.6	50.6	1.4	1.6
13	22.5	0.013	0.013	0.01	0.003	0.020	3.1	0.01	0.003	0.020	3.1	0.6	0.3	−3.7	0.3	0.5	−2.9
12	45.0	−0.015	−0.015	0.01	0.002	0.016	2.5	0.01	0.002	0.016	2.5	0.2	0.0	−1.5	−0.1	0.2	−0.7
12	45.0	−0.009	−0.005	29.91	0.143	1.041	157.1	30.50	0.144	1.051	158.7	47.8	14.4	−49.8	24.5	1.1	4.5
12	45.0	−0.004	−0.002	60.05	0.204	1.468	224.1	61.23	0.206	1.482	226.2	98.1	28.6	−106.7	49.4	1.0	9.5
12	45.0	−2.030	−2.101	60.91	0.205	1.477	225.8	62.28	0.207	1.494	228.3	99.0	−19.3	−126.6	51.4	−45.5	−13.7
12	45.0	0.024	0.026	60.00	0.203	1.465	224.1	61.17	0.205	1.480	226.3	97.7	28.7	−105.8	49.0	1.1	10.4
12	45.0	2.023	2.099	60.67	0.205	1.473	225.4	62.02	0.207	1.489	227.9	100.1	77.9	−79.8	50.3	48.7	39.9
12	45.0	3.984	4.134	60.90	0.205	1.475	225.9	62.38	0.208	1.493	228.6	107.6	128.9	−57.7	56.1	96.5	65.6
12	45.0	5.999	6.222	61.15	0.206	1.478	226.3	62.74	0.208	1.497	229.3	120.5	184.5	−37.8	66.1	145.3	89.5
12	45.0	2.020	2.097	60.53	0.204	1.471	225.2	61.89	0.207	1.487	227.7	100.1	78.1	−79.3	50.3	48.9	40.4
12	45.0	−0.035	−0.035	59.85	0.203	1.462	223.9	61.01	0.205	1.476	226.1	97.2	27.6	−105.1	48.6	0.1	11.0
12	45.0	−0.046	−0.046	0.01	0.003	0.021	3.2	0.01	0.003	0.022	3.3	0.7	0.2	−3.0	0.4	0.4	−2.2
11	67.5	0.030	0.030	0.00	0.001	0.005	0.7	0.00	0.001	0.005	0.7	0.0	0.0	0.0	−0.3	0.2	0.8
11	67.5	0.035	0.059	30.17	0.143	1.047	157.7	30.79	0.145	1.058	159.3	48.7	20.9	−46.9	25.4	7.6	7.5
11	67.5	0.041	0.060	59.87	0.203	1.469	223.5	61.11	0.205	1.484	225.8	96.6	39.2	−99.6	47.9	11.6	16.6
11	67.5	−2.005	−2.051	60.63	0.205	1.476	225.1	61.98	0.207	1.492	227.6	98.4	−2.6	−121.6	50.8	−28.9	−8.7
11	67.5	−0.030	−0.013	59.80	0.203	1.465	223.6	61.04	0.205	1.480	225.9	96.5	37.9	−100.6	47.8	10.4	15.5
11	67.5	1.998	2.084	60.13	0.204	1.468	224.3	61.46	0.206	1.484	226.8	100.0	82.6	−77.4	50.2	53.6	42.2
11	67.5	4.015	4.169	59.99	0.203	1.466	224.1	61.42	0.206	1.483	226.7	107.9	127.7	−61.5	56.4	95.3	61.9
11	67.5	5.959	6.176	60.33	0.204	1.470	224.7	61.87	0.207	1.488	227.5	121.2	174.8	−50.7	66.9	135.8	76.6
11	67.5	1.970	2.054	60.53	0.204	1.472	225.1	61.88	0.207	1.488	227.6	100.4	82.2	−78.1	50.6	53.2	41.5
11	67.5	−0.003	0.016	59.68	0.203	1.461	223.5	60.91	0.205	1.476	225.8	97.0	38.9	−101.0	48.3	11.3	15.2
11	67.5	−0.014	−0.014	0.00	0.000	0.000	0.0	0.00	0.000	0.000	0.0	0.6	0.2	−1.9	0.0	0.4	−1.1

Table C.7: Summary of data for Configuration 6

				Tunnel Condition								Force And Moment Data					
	Model Orientation			Uncorrected				Corrected				Uncorrected			Corrected		
Run	ψ (deg)	$\alpha_{s,u}$ (deg)	$\alpha_{s,c}$ (deg)	q_u (lb/ft^2)	M_u	$Re_u \times 10^6$	v_u (ft/s)	q_c (lb/ft^2)	M_c	$Re_c \times 10^6$	v_c (ft/s)	D_u (lb)	L_u (lb)	PM_u (ft lb)	D_c (lb)	L_c (lb)	PM_c (ft lb)
7	0.0	0.024	0.024	0.00	0.000	0.000	0.0	0.00	0.000	0.000	0.0	0.0	0.0	−0.1	0.0	0.3	0.7
7	0.0	0.027	0.040	10.00	0.082	0.589	91.3	10.25	0.083	0.596	92.4	19.8	5.8	−13.5	12.3	1.4	4.2
7	0.0	0.025	0.038	9.98	0.082	0.588	91.2	10.22	0.083	0.596	92.3	19.9	5.7	−13.5	12.3	1.4	4.2
7	0.0	0.029	0.041	19.99	0.116	0.831	129.4	20.47	0.118	0.841	131.0	40.8	11.5	−30.8	25.6	2.6	4.7
7	0.0	0.039	0.049	30.23	0.143	1.020	159.5	30.96	0.145	1.032	161.4	61.4	16.4	−48.4	38.1	3.2	6.0
7	0.0	0.034	0.042	40.16	0.165	1.173	184.3	41.14	0.167	1.187	186.5	81.8	21.9	−65.8	50.4	3.6	8.5
7	0.0	0.051	0.057	50.82	0.187	1.317	207.8	52.06	0.189	1.333	210.3	104.3	26.7	−87.0	63.8	3.5	9.2
7	0.0	0.028	0.036	59.86	0.203	1.427	226.0	61.32	0.205	1.444	228.7	123.7	32.0	−105.0	75.0	4.4	11.2
7	0.0	0.031	0.040	70.18	0.220	1.542	245.3	71.88	0.223	1.560	248.2	144.6	38.4	−123.9	86.8	6.3	14.6
7	0.0	0.034	0.041	60.05	0.203	1.426	226.6	61.52	0.206	1.443	229.3	123.9	32.4	−105.3	75.2	4.8	10.9
7	0.0	−0.987	−1.002	60.12	0.203	1.427	226.7	61.60	0.206	1.444	229.4	124.2	17.7	−109.5	76.0	−9.3	4.9
7	0.0	−2.033	−2.073	60.30	0.204	1.429	227.0	61.83	0.206	1.447	229.9	125.4	1.2	−114.8	77.8	−25.0	−2.0
7	0.0	0.010	0.017	60.08	0.203	1.426	226.6	61.54	0.206	1.443	229.3	123.7	31.8	−105.7	75.1	4.3	10.5
7	0.0	0.949	0.978	59.64	0.203	1.421	225.7	61.11	0.205	1.439	228.5	125.1	46.2	−99.5	75.9	18.0	18.3
7	0.0	2.003	2.057	60.28	0.204	1.429	227.0	61.80	0.206	1.447	229.8	127.3	62.3	−93.3	77.4	33.2	26.4
7	0.0	2.933	3.006	60.05	0.203	1.426	226.5	61.60	0.206	1.444	229.4	130.1	76.2	−88.7	79.5	45.8	32.6
7	0.0	4.021	4.119	59.96	0.203	1.425	226.4	61.55	0.206	1.444	229.4	134.4	93.3	−84.5	82.6	60.8	38.9
7	0.0	5.032	5.153	59.73	0.203	1.422	225.9	61.34	0.206	1.441	229.0	139.9	110.4	−81.0	86.8	75.0	44.4
7	0.0	5.951	6.092	59.86	0.203	1.423	226.2	61.51	0.206	1.443	229.3	145.0	126.3	−76.3	90.5	87.3	50.9
7	0.0	2.030	2.084	60.15	0.204	1.427	226.8	61.67	0.206	1.444	229.6	127.1	62.5	−92.9	77.3	33.4	26.9
7	0.0	−0.035	−0.028	59.90	0.203	1.424	226.3	61.36	0.206	1.441	229.0	123.5	31.6	−105.3	74.8	4.0	10.8
7	0.0	−0.060	−0.060	0.01	0.002	0.017	2.7	0.01	0.002	0.017	2.7	0.4	0.4	−1.3	0.1	0.6	−0.5
8	22.5	−0.062	−0.062	0.00	0.000	0.000	0.0	0.00	0.000	0.000	0.0	0.3	0.2	−3.2	0.0	0.4	−2.4
8	22.5	−0.058	−0.067	30.04	0.143	1.012	159.3	30.78	0.145	1.025	161.2	62.6	10.4	−56.1	39.3	−2.9	−1.8
8	22.5	−0.032	−0.039	59.99	0.203	1.423	226.6	61.46	0.206	1.441	229.3	125.3	23.2	−113.6	76.6	−4.4	2.4
8	22.5	−1.967	−2.035	60.53	0.204	1.427	227.8	62.08	0.207	1.445	230.7	125.8	−17.0	−126.8	78.2	−43.3	−13.9
8	22.5	−0.008	−0.014	59.47	0.202	1.413	225.9	60.93	0.205	1.430	228.6	124.5	24.2	−112.1	75.9	−3.4	4.0
8	22.5	1.986	2.042	59.93	0.203	1.417	226.8	61.47	0.206	1.435	229.7	128.0	64.4	−94.5	78.2	35.3	25.1
8	22.5	3.957	4.073	59.57	0.203	1.412	226.2	61.20	0.205	1.431	229.2	133.6	104.7	−75.8	82.0	72.4	47.5
8	22.5	6.020	6.198	59.82	0.203	1.415	226.7	61.56	0.206	1.435	230.0	144.6	150.7	−60.3	90.0	111.4	67.1
8	22.5	2.044	2.102	60.26	0.204	1.420	227.5	61.81	0.206	1.438	230.4	128.3	65.8	−94.3	78.5	36.6	25.4
8	22.5	−0.045	−0.052	60.08	0.203	1.418	227.2	61.55	0.206	1.435	229.9	125.3	23.3	−113.2	76.6	−4.3	2.9
8	22.5	−0.058	−0.058	0.01	0.003	0.018	2.8	0.01	0.003	0.018	2.8	0.5	0.5	−4.3	0.3	0.7	−3.5
9	45.0	−0.059	−0.059	0.00	0.001	0.011	1.7	0.00	0.002	0.011	1.7	0.1	0.4	−3.1	−0.1	0.6	−2.3
9	45.0	−0.047	−0.048	30.14	0.143	1.011	159.8	30.83	0.145	1.022	161.6	60.0	13.3	−50.9	36.7	0.0	3.4
9	45.0	−0.048	−0.049	60.00	0.203	1.419	226.9	61.38	0.206	1.435	229.5	120.1	26.6	−105.0	71.4	−1.0	11.1
9	45.0	−2.027	−2.096	61.05	0.205	1.429	229.0	62.64	0.208	1.447	232.0	121.1	−18.6	−130.2	73.5	−44.9	−17.4
9	45.0	0.007	0.007	60.33	0.204	1.420	227.7	61.72	0.206	1.436	230.3	119.8	27.5	−104.0	71.2	−0.1	12.1
9	45.0	2.025	2.099	60.45	0.204	1.420	228.0	62.03	0.207	1.439	231.0	122.6	76.9	−73.1	72.8	47.8	46.6
9	45.0	3.997	4.143	60.45	0.204	1.420	228.0	62.14	0.207	1.440	231.2	130.9	126.3	−48.7	79.4	93.8	74.7
9	45.0	6.042	6.255	60.88	0.205	1.424	228.9	62.70	0.208	1.446	232.3	143.9	177.7	−23.8	89.4	138.3	103.6
9	45.0	1.975	2.048	60.69	0.205	1.422	228.5	62.27	0.207	1.441	231.5	122.2	75.8	−72.3	72.3	46.8	47.3
9	45.0	−0.026	−0.027	60.27	0.204	1.417	227.7	61.66	0.206	1.433	230.3	119.6	27.0	−102.8	70.9	−0.6	13.4
9	45.0	−0.033	−0.033	0.01	0.002	0.017	2.7	0.01	0.002	0.017	2.7	0.6	0.5	−4.5	0.3	0.7	−3.7
10	67.5	−0.033	−0.033	0.01	0.002	0.015	2.4	0.01	0.002	0.015	2.4	0.1	0.2	−2.1	−0.2	0.4	−1.3
10	67.5	−0.040	−0.025	30.18	0.143	1.012	159.9	30.90	0.145	1.024	161.7	59.6	18.0	−48.9	36.3	4.7	5.4
10	67.5	−0.021	−0.010	60.03	0.203	1.419	227.0	61.44	0.206	1.436	229.6	118.7	34.6	−104.2	70.0	7.0	11.9
10	67.5	−1.960	−2.008	60.81	0.205	1.426	228.6	62.38	0.207	1.444	231.5	119.7	−4.0	−126.9	72.1	−30.3	−13.9
10	67.5	−0.036	−0.026	59.88	0.203	1.415	226.8	61.30	0.205	1.431	229.5	118.6	33.8	−105.0	69.9	6.3	11.1
10	67.5	2.010	2.086	60.20	0.204	1.418	227.5	61.75	0.206	1.436	230.4	121.2	76.5	−76.6	71.4	47.4	43.1
10	67.5	4.001	4.143	59.34	0.202	1.408	225.8	60.97	0.205	1.427	228.9	128.4	119.9	−57.7	76.8	87.5	65.7
10	67.5	5.981	6.186	59.60	0.203	1.411	226.3	61.33	0.206	1.431	229.6	140.4	166.4	−45.1	86.0	127.3	82.2
10	67.5	2.030	2.108	60.21	0.204	1.418	227.5	61.77	0.206	1.436	230.4	121.3	78.2	−74.8	71.5	49.0	44.9
10	67.5	−0.014	−0.002	59.98	0.203	1.415	227.0	61.39	0.206	1.432	229.7	118.8	35.2	−103.4	70.2	7.7	12.7
10	67.5	−0.015	−0.015	0.01	0.002	0.013	2.1	0.01	0.002	0.014	2.1	0.6	0.4	−3.9	0.3	0.6	−3.1

Table C.8: Summary of data for Configuration 7

	Model Orientation			Tunnel Condition								Force And Moment Data					
				Uncorrected				Corrected				Uncorrected			Corrected		
Run	ψ (deg)	$\alpha_{s,u}$ (deg)	$\alpha_{s,c}$ (deg)	q_u (lb/ft^2)	M_u	$Re_u \times 10^6$	v_u (ft/s)	q_c (lb/ft^2)	M_c	$Re_c \times 10^6$	v_c (ft/s)	D_u (lb)	L_u (lb)	PM_u (ft lb)	D_c (lb)	L_c (lb)	PM_c (ft lb)
6	0.0	−0.017	−0.017	0.01	0.002	0.017	2.6	0.01	0.002	0.017	2.6	0.0	0.3	0.7	−0.3	0.5	1.5
6	0.0	−0.011	−0.016	30.39	0.144	1.028	159.6	31.07	0.145	1.040	161.3	59.6	11.4	−51.7	36.3	−1.9	2.6
6	0.0	−0.003	−0.010	61.02	0.205	1.446	227.8	62.39	0.207	1.462	230.4	121.0	22.8	−112.4	72.3	−4.8	3.7
6	0.0	−2.011	−2.050	60.72	0.204	1.440	227.4	62.12	0.207	1.457	230.0	120.4	1.1	−110.8	72.8	−25.2	2.0
6	0.0	0.042	0.035	59.96	0.203	1.430	226.0	61.30	0.205	1.446	228.5	118.9	23.2	−109.7	70.2	−4.4	6.5
6	0.0	1.972	1.994	59.91	0.203	1.429	225.9	61.29	0.205	1.446	228.5	120.7	43.2	−106.0	70.8	14.1	13.6
6	0.0	3.992	4.042	59.69	0.203	1.427	225.5	61.11	0.205	1.443	228.2	124.6	64.4	−104.9	72.9	32.0	18.5
6	0.0	6.053	6.123	59.55	0.202	1.424	225.3	61.00	0.205	1.442	228.0	132.1	84.3	−105.0	77.2	44.9	22.4
6	0.0	1.966	1.988	60.04	0.203	1.430	226.2	61.42	0.206	1.446	228.8	120.4	43.2	−105.6	70.5	14.1	13.9
6	0.0	0.044	0.036	59.87	0.203	1.427	225.9	61.21	0.205	1.443	228.5	118.9	22.8	−110.1	70.2	−4.8	6.1
6	0.0	0.029	0.029	0.01	0.002	0.015	2.4	0.01	0.002	0.015	2.4	0.6	0.3	−1.5	0.3	0.5	−0.7

Table C.9: Summary of data for Configuration 8

	Model Orientation			Tunnel Condition								Force And Moment Data					
				Uncorrected				Corrected				Uncorrected			Corrected		
Run	ψ (deg)	$\alpha_{s,u}$ (deg)	$\alpha_{s,c}$ (deg)	q_u (lb/ft^2)	M_u	$Re_u \times 10^6$	v_u (ft/s)	q_c (lb/ft^2)	M_c	$Re_c \times 10^6$	v_c (ft/s)	D_u (lb)	L_u (lb)	PM_u (ft lb)	D_c (lb)	L_c (lb)	PM_c (ft lb)
40	0.0	−0.005	−0.005	0.01	0.003	0.019	2.9	0.01	0.003	0.019	2.9	0.1	17.9	0.0	−0.2	18.1	0.8
40	0.0	0.001	0.102	30.15	0.144	1.020	159.6	30.74	0.145	1.030	161.1	40.0	44.8	−46.2	16.8	31.5	8.2
40	0.0	0.005	0.074	60.20	0.204	1.433	227.1	61.38	0.206	1.447	229.3	81.7	70.2	−101.6	33.1	42.6	14.6
40	0.0	−2.049	−2.049	59.81	0.204	1.426	226.5	61.06	0.206	1.441	228.8	80.6	26.5	−120.9	33.0	0.2	−8.2
40	0.0	0.042	0.114	59.97	0.204	1.427	226.9	61.15	0.206	1.441	229.1	81.6	72.1	−102.4	33.0	44.6	13.9
40	0.0	2.037	2.177	60.07	0.204	1.428	227.1	61.32	0.206	1.443	229.4	85.9	115.6	−85.6	36.2	86.5	34.1
40	0.0	3.959	4.139	60.69	0.205	1.435	228.3	62.04	0.208	1.450	230.8	93.9	144.8	−72.0	42.5	112.5	51.3
40	0.0	6.043	6.274	60.91	0.206	1.437	228.7	62.37	0.208	1.454	231.5	105.6	184.6	−56.8	51.2	145.2	70.6
40	0.0	1.957	2.097	59.90	0.204	1.425	226.8	61.14	0.206	1.439	229.2	85.6	115.4	−86.1	35.9	86.3	33.5
40	0.0	−0.015	0.057	59.90	0.204	1.425	226.8	61.07	0.206	1.438	229.0	81.4	71.9	−102.6	32.8	44.4	13.5
40	0.0	−0.007	0.053	89.64	0.251	1.735	279.2	91.40	0.254	1.752	282.0	124.0	97.0	−160.3	47.2	55.8	25.0
40	0.0	−0.022	−0.022	0.01	0.003	0.022	3.5	0.01	0.003	0.023	3.6	0.6	19.2	−2.1	0.3	19.4	−1.3
38	22.5	0.012	0.012	0.00	0.001	0.008	1.3	0.00	0.001	0.008	1.3	0.1	1.0	0.6	−0.2	1.2	1.4
38	22.5	0.016	0.055	30.40	0.144	1.009	161.2	31.00	0.146	1.018	162.8	40.2	25.5	−46.4	16.8	12.2	8.0
38	22.5	0.020	0.049	59.91	0.204	1.410	227.7	61.09	0.206	1.424	230.0	80.7	45.8	−94.8	32.0	18.2	21.4
38	22.5	−2.010	−2.061	60.90	0.206	1.420	229.7	62.20	0.208	1.436	232.2	81.4	−6.3	−110.4	33.7	−32.6	2.5
38	22.5	0.019	0.049	60.27	0.205	1.412	228.6	61.46	0.207	1.426	230.8	81.2	46.2	−96.0	32.5	18.6	20.2
38	22.5	1.981	2.091	60.48	0.205	1.414	229.0	61.77	0.207	1.429	231.4	83.7	98.4	−81.3	34.0	69.3	38.3
38	22.5	3.960	4.150	60.90	0.206	1.419	229.8	62.32	0.208	1.435	232.5	90.7	153.3	−67.5	39.3	120.9	55.8
38	22.5	5.969	6.225	61.33	0.206	1.424	230.7	62.86	0.209	1.441	233.5	103.6	203.1	−59.6	49.5	164.0	67.7
38	22.5	2.034	2.147	60.16	0.204	1.410	228.4	61.45	0.206	1.425	230.9	84.1	100.0	−81.2	34.3	70.9	38.5
38	22.5	0.008	0.037	60.21	0.204	1.410	228.5	61.40	0.206	1.424	230.8	81.1	45.8	−95.6	32.4	18.2	20.5
38	22.5	0.008	0.038	90.03	0.252	1.718	281.1	91.81	0.254	1.735	283.9	124.0	69.0	−148.9	47.2	27.8	36.4
38	22.5	−0.002	−0.002	0.02	0.003	0.024	3.8	0.02	0.003	0.024	3.9	0.6	1.3	−1.2	0.3	1.5	−0.4
37	45.0	−0.042	−0.042	0.01	0.003	0.020	3.1	0.01	0.003	0.020	3.1	0.4	1.1	−1.4	0.1	1.3	−0.6
37	45.0	−0.041	0.014	30.12	0.144	1.005	160.5	30.68	0.145	1.014	162.0	40.1	30.8	−44.9	16.8	17.5	9.5
37	45.0	−0.033	0.007	60.27	0.205	1.414	228.5	61.40	0.206	1.428	230.6	81.3	53.1	−92.9	32.7	25.6	23.2
37	45.0	−2.000	−2.032	60.80	0.205	1.419	229.6	62.11	0.208	1.434	232.1	81.4	5.7	−117.1	33.8	−20.6	−4.3
37	45.0	0.035	0.077	60.58	0.205	1.415	229.3	61.70	0.207	1.428	231.4	81.5	54.2	−92.8	32.8	26.6	23.4
37	45.0	1.977	2.091	60.66	0.205	1.416	229.4	61.98	0.207	1.431	231.9	85.1	102.0	−69.4	35.3	72.9	50.2
37	45.0	4.003	4.196	61.07	0.206	1.420	230.2	62.52	0.208	1.437	233.0	92.6	156.9	−48.6	41.2	124.4	74.8
37	45.0	5.971	6.236	61.15	0.206	1.421	230.4	62.71	0.209	1.439	233.3	104.2	210.7	−31.6	50.2	171.6	95.7
37	45.0	2.000	2.115	60.78	0.205	1.417	229.7	62.10	0.208	1.432	232.2	85.3	102.5	−69.7	35.5	73.5	50.0
37	45.0	0.025	0.068	60.41	0.205	1.412	229.0	61.54	0.207	1.425	231.1	81.7	54.6	−93.0	33.0	27.1	23.2
37	45.0	0.030	0.078	90.48	0.253	1.723	281.9	92.16	0.255	1.739	284.5	124.2	87.4	−150.4	47.3	46.2	35.0
37	45.0	0.013	0.013	0.00	0.002	0.012	2.0	0.00	0.002	0.013	2.0	0.6	1.3	−2.3	0.3	1.5	−1.5
36	67.5	−0.032	−0.032	0.00	0.000	0.000	0.0	0.00	0.000	0.000	0.0	0.1	0.0	−0.4	NaN	0.2	0.4
36	67.5	−0.030	−0.001	30.04	0.143	1.003	160.3	30.62	0.145	1.012	161.9	39.3	22.1	−42.0	16.0	8.8	12.3
36	67.5	−0.027	−0.005	60.44	0.205	1.415	228.9	61.62	0.207	1.428	231.1	79.5	41.3	−87.7	30.8	13.7	28.4
36	67.5	−2.023	−2.079	60.49	0.205	1.414	229.1	61.79	0.207	1.429	231.6	80.0	−8.9	−113.7	32.4	−35.2	−0.9
36	67.5	−0.006	0.017	60.06	0.204	1.408	228.3	61.23	0.206	1.422	230.5	79.5	41.8	−87.4	30.8	14.3	28.8
36	67.5	2.044	2.155	60.35	0.205	1.411	228.9	61.64	0.207	1.426	231.4	82.2	98.0	−61.6	32.4	68.9	58.2
36	67.5	3.982	4.175	61.13	0.206	1.420	230.5	62.55	0.208	1.436	233.1	89.5	154.5	−40.2	38.1	122.1	83.1
36	67.5	6.008	6.282	61.44	0.207	1.423	231.1	62.98	0.209	1.441	233.9	101.3	213.9	−21.6	47.3	174.7	105.7
36	67.5	1.960	2.068	60.48	0.205	1.412	229.2	61.77	0.207	1.427	231.6	82.4	96.7	−62.3	32.7	67.6	57.3
36	67.5	−0.033	−0.009	59.90	0.204	1.405	228.1	61.07	0.206	1.419	230.3	79.7	42.3	−87.6	31.1	14.7	28.5
36	67.5	−0.033	−0.004	90.07	0.252	1.717	281.4	91.83	0.254	1.733	284.2	121.5	68.5	−139.0	44.7	27.3	46.2
36	67.5	−0.042	−0.042	0.01	0.003	0.019	3.0	0.01	0.003	0.019	3.0	0.6	1.2	−2.1	0.3	1.4	−1.3

Table C.10: Summary of data for Configuration 9

				Tunnel Condition								Force And Moment Data					
	Model Orientation			Uncorrected				Corrected				Uncorrected			Corrected		
Run	ψ (deg)	$\alpha_{s,u}$ (deg)	$\alpha_{s,c}$ (deg)	q_u (lb/ft^2)	M_u	$Re_u \times 10^6$	v_u (ft/s)	q_c (lb/ft^2)	M_c	$Re_c \times 10^6$	v_c (ft/s)	D_u (lb)	L_u (lb)	PM_u (ft lb)	D_c (lb)	L_c (lb)	PM_c (ft lb)
41	0.0	−0.038	−0.038	0.00	0.002	0.011	1.8	0.00	0.002	0.011	1.8	0.0	0.0	0.0	−0.3	0.2	0.8
41	0.0	−0.035	−0.017	30.14	0.144	1.019	159.6	30.67	0.145	1.028	161.0	39.0	19.1	−50.8	15.7	5.8	3.5
41	0.0	−0.032	−0.016	60.12	0.204	1.431	227.0	61.18	0.206	1.444	229.0	79.4	37.7	−108.7	30.7	10.1	7.4
41	0.0	−2.005	−2.031	60.43	0.205	1.433	227.7	61.54	0.207	1.446	229.8	77.8	10.1	−114.1	30.2	−16.2	−1.3
41	0.0	0.024	0.041	59.52	0.203	1.420	226.1	60.57	0.205	1.433	228.1	79.0	38.4	−107.6	30.3	10.8	8.6
41	0.0	1.945	2.003	59.74	0.204	1.422	226.5	60.84	0.206	1.435	228.6	81.8	65.7	−100.2	32.0	36.6	19.4
41	0.0	4.039	4.135	60.28	0.205	1.427	227.7	61.45	0.207	1.441	229.9	88.6	94.3	−96.5	36.9	61.7	27.0
41	0.0	6.008	6.131	60.62	0.205	1.431	228.3	61.85	0.207	1.445	230.6	97.5	118.4	−93.2	42.7	79.2	34.1
41	0.0	1.969	2.027	60.03	0.204	1.424	227.2	61.13	0.206	1.437	229.3	82.5	66.1	−101.4	32.7	37.1	18.2
41	0.0	0.022	0.039	59.63	0.203	1.419	226.5	60.69	0.205	1.431	228.5	78.9	38.5	−107.6	30.2	11.0	8.6
41	0.0	0.019	0.038	90.24	0.252	1.737	280.4	91.83	0.254	1.752	282.9	121.5	59.2	−169.4	44.7	18.0	16.0
41	0.0	0.013	0.013	0.00	0.000	0.000	0.0	0.00	0.000	0.000	0.0	0.7	0.4	−2.8	0.0	0.6	−2.0
42	22.5	0.013	0.013	0.00	0.000	0.000	0.0	0.00	0.000	0.000	0.0	0.0	0.0	0.0	0.0	0.3	0.8
42	22.5	0.017	0.032	30.06	0.143	1.012	159.8	30.61	0.145	1.021	161.2	39.4	18.2	−48.7	16.1	4.9	5.6
42	22.5	0.018	0.029	60.50	0.205	1.429	228.2	61.60	0.207	1.442	230.2	80.6	34.6	−101.2	31.9	7.0	14.9
42	22.5	−1.963	−1.992	60.86	0.206	1.432	229.0	62.02	0.208	1.445	231.1	80.1	7.6	−106.7	32.4	−18.8	6.2
42	22.5	0.043	0.054	60.27	0.205	1.424	227.9	61.37	0.207	1.437	230.0	80.7	34.7	−101.9	32.0	7.1	14.3
42	22.5	2.039	2.094	60.22	0.205	1.423	227.8	61.36	0.206	1.436	230.0	83.5	64.3	−97.1	33.6	35.1	22.7
42	22.5	3.994	4.083	60.57	0.205	1.426	228.5	61.79	0.207	1.441	230.8	89.1	90.1	−91.2	37.4	57.7	32.2
42	22.5	6.010	6.128	61.10	0.206	1.432	229.6	62.41	0.208	1.447	232.0	99.3	116.2	−85.7	44.6	76.9	41.6
42	22.5	2.017	2.072	60.05	0.204	1.420	227.6	61.19	0.206	1.433	229.7	83.7	63.8	−97.8	33.8	34.7	21.8
42	22.5	0.034	0.045	59.61	0.203	1.414	226.7	60.69	0.205	1.427	228.8	80.7	34.8	−102.0	32.0	7.2	14.2
42	22.5	0.028	0.058	89.46	0.251	1.724	279.6	91.09	0.253	1.739	282.1	127.0	69.4	−167.1	50.2	28.2	18.3
42	22.5	0.029	0.029	0.02	0.003	0.023	3.7	0.02	0.003	0.023	3.7	0.3	0.0	−0.9	0.0	0.2	−0.1
43	45.0	0.028	0.028	0.00	0.000	0.000	0.0	0.00	0.000	0.000	0.0	0.0	0.0	0.3	0.0	0.2	1.1
43	45.0	0.029	0.045	30.14	0.144	1.012	160.0	30.66	0.145	1.021	161.4	40.3	18.2	−47.9	17.0	4.9	6.5
43	45.0	0.036	0.049	59.80	0.204	1.420	226.8	60.83	0.206	1.432	228.8	80.9	35.7	−102.1	32.2	8.1	14.1
43	45.0	−2.010	−2.039	60.50	0.205	1.425	228.4	61.64	0.207	1.439	230.5	80.8	7.6	−109.2	33.1	−18.6	3.7
43	45.0	−0.016	−0.003	59.92	0.204	1.418	227.3	60.95	0.206	1.430	229.2	81.0	35.4	−103.3	32.4	7.8	12.8
43	45.0	2.017	2.078	59.78	0.204	1.416	227.1	60.91	0.206	1.429	229.2	83.3	67.4	−97.1	33.5	38.3	22.6
43	45.0	4.002	4.109	60.07	0.204	1.419	227.6	61.29	0.206	1.433	229.9	88.3	101.0	−93.5	36.7	68.5	29.9
43	45.0	6.026	6.174	60.59	0.205	1.424	228.7	61.90	0.207	1.440	231.1	97.2	135.0	−92.8	42.5	95.7	34.6
43	45.0	1.994	2.055	59.79	0.204	1.415	227.1	60.92	0.206	1.428	229.3	83.6	67.8	−97.7	33.7	38.7	22.0
43	45.0	0.015	0.032	59.96	0.204	1.417	227.5	60.99	0.206	1.429	229.4	81.9	37.9	−104.8	33.2	10.3	11.4
43	45.0	0.023	0.047	90.82	0.253	1.734	281.9	92.39	0.255	1.749	284.3	126.8	64.2	−167.7	49.9	23.0	17.7
43	45.0	0.010	0.010	0.00	0.001	0.007	1.1	0.00	0.001	0.007	1.1	0.5	0.2	−1.3	0.2	0.5	−0.5
44	67.5	0.010	0.010	0.00	0.000	0.000	0.0	0.00	0.000	0.000	0.0	0.0	0.0	0.1	0.0	0.2	0.9
44	67.5	0.016	0.042	30.15	0.144	1.010	160.2	30.68	0.145	1.019	161.6	39.9	21.6	−51.6	16.5	8.3	2.8
44	67.5	0.022	0.039	60.07	0.204	1.420	227.6	61.12	0.206	1.432	229.6	80.4	37.8	−106.3	31.7	10.2	9.9
44	67.5	−2.028	−2.052	60.84	0.206	1.426	229.3	61.98	0.208	1.439	231.4	80.5	11.2	−108.1	32.9	−15.1	4.7
44	67.5	0.019	0.035	60.07	0.204	1.415	227.9	61.12	0.206	1.428	229.9	80.5	37.9	−106.4	31.8	10.3	9.8
44	67.5	2.002	2.057	59.80	0.204	1.412	227.4	60.92	0.206	1.425	229.5	82.6	64.3	−104.2	32.8	35.2	15.4
44	67.5	4.026	4.124	59.88	0.204	1.412	227.6	61.09	0.206	1.426	229.9	88.4	94.8	−105.6	36.7	62.3	17.9
44	67.5	6.044	6.181	60.77	0.206	1.422	229.3	62.06	0.208	1.437	231.7	96.9	127.6	−102.5	42.1	88.2	24.9
44	67.5	2.023	2.080	59.98	0.204	1.413	227.8	61.10	0.206	1.426	229.9	83.2	65.0	−105.2	33.3	35.8	14.5
44	67.5	0.026	0.044	59.77	0.204	1.410	227.4	60.81	0.206	1.423	229.4	80.7	38.6	−106.6	32.0	11.1	9.6
44	67.5	0.047	0.072	90.00	0.252	1.723	280.8	91.57	0.254	1.738	283.3	122.3	64.7	−172.9	45.4	23.5	12.6
44	67.5	0.034	0.034	0.01	0.002	0.015	2.5	0.01	0.002	0.016	2.5	−0.2	0.2	0.8	−0.5	0.4	1.6

Table C.11: Summary of data for Configuration 10

				Tunnel Condition								Force And Moment Data					
	Model Orientation			Uncorrected				Corrected				Uncorrected			Corrected		
Run	ψ (deg)	$\alpha_{s,u}$ (deg)	$\alpha_{s,c}$ (deg)	q_u (lb/ft^2)	M_u	$Re_u \times 10^6$	v_u (ft/s)	q_c (lb/ft^2)	M_c	$Re_c \times 10^6$	v_c (ft/s)	D_u (lb)	L_u (lb)	PM_u (ft lb)	D_c (lb)	L_c (lb)	PM_c (ft lb)
31	0.0	0.009	0.009	0.00	0.002	0.013	2.0	0.00	0.002	0.013	2.0	0.0	0.3	−1.5	−0.3	0.5	−0.7
31	0.0	0.014	0.052	30.06	0.143	1.005	160.0	30.64	0.144	1.015	161.5	43.9	24.9	−49.1	20.6	11.6	5.2
31	0.0	0.017	0.051	60.41	0.204	1.416	228.4	61.59	0.206	1.430	230.6	89.9	48.2	−104.5	41.3	20.7	11.7
31	0.0	−1.952	−1.968	60.37	0.204	1.415	228.3	61.62	0.206	1.430	230.7	89.4	16.3	−114.0	41.7	−10.0	−1.0
31	0.0	−0.017	0.016	59.96	0.204	1.411	227.5	61.14	0.206	1.424	229.7	89.7	47.6	−105.0	41.1	20.0	11.1
31	0.0	1.977	2.059	60.25	0.204	1.414	228.1	61.50	0.206	1.428	230.4	94.3	79.5	−94.6	44.5	50.4	25.0
31	0.0	4.029	4.157	59.70	0.203	1.407	227.1	61.02	0.205	1.422	229.6	103.1	111.2	−88.1	51.4	78.7	35.3
31	0.0	6.013	6.184	59.77	0.203	1.408	227.2	61.19	0.206	1.425	229.8	114.4	144.6	−77.1	59.8	105.3	50.3
31	0.0	1.971	2.053	60.01	0.204	1.411	227.6	61.26	0.206	1.425	230.0	94.3	79.8	−94.4	44.5	50.7	25.2
31	0.0	0.005	0.039	59.85	0.203	1.409	227.3	61.02	0.205	1.422	229.6	89.9	48.4	−104.5	41.2	20.8	11.7
31	0.0	−0.004	−0.004	0.02	0.004	0.026	4.1	0.02	0.004	0.026	4.1	0.2	0.6	−1.9	−0.1	0.8	−1.1
30	45.0	0.019	0.019	0.00	0.001	0.005	0.7	0.00	0.001	0.005	0.8	0.0	0.2	−1.3	−0.2	0.4	−0.5
30	45.0	0.024	0.049	30.00	0.143	1.008	159.6	30.55	0.144	1.017	161.0	42.0	21.1	−42.5	18.7	7.8	11.8
30	45.0	0.031	0.052	60.26	0.204	1.418	227.9	61.38	0.206	1.431	230.0	86.3	40.8	−89.2	37.6	13.2	27.0
30	45.0	−2.048	−2.102	60.94	0.205	1.424	229.3	62.26	0.207	1.439	231.8	86.7	−8.4	−108.2	39.1	−34.7	4.6
30	45.0	−0.053	−0.035	60.29	0.204	1.415	228.1	61.40	0.206	1.428	230.2	85.9	39.0	−88.9	37.3	11.5	27.1
30	45.0	2.000	2.096	60.30	0.204	1.414	228.2	61.60	0.206	1.429	230.7	89.6	90.3	−67.9	39.8	61.2	51.7
30	45.0	3.985	4.157	60.38	0.204	1.415	228.4	61.81	0.207	1.431	231.1	97.5	142.4	−48.8	46.0	110.0	74.6
30	45.0	5.949	6.193	60.36	0.204	1.414	228.4	61.89	0.207	1.432	231.2	109.4	195.5	−26.6	55.3	156.6	100.6
30	45.0	2.005	2.101	60.43	0.204	1.415	228.5	61.74	0.207	1.430	231.0	89.5	90.4	−67.3	39.7	61.3	52.3
30	45.0	0.017	0.038	59.90	0.203	1.408	227.5	61.01	0.205	1.421	229.6	85.8	40.6	−88.6	37.1	13.0	27.6

Table C.12: Summary of data for Configuration 11

				Tunnel Condition								Force And Moment Data					
	Model Orientation			Uncorrected				Corrected				Uncorrected			Corrected		
Run	ψ (deg)	$\alpha_{s,u}$ (deg)	$\alpha_{s,c}$ (deg)	q_u (lb/ft^2)	M_u	$Re_u \times 10^6$	v_u (ft/s)	q_c (lb/ft^2)	M_c	$Re_c \times 10^6$	v_c (ft/s)	D_u (lb)	L_u (lb)	PM_u (ft lb)	D_c (lb)	L_c (lb)	PM_c (ft lb)
32	0.0	−0.004	−0.004	0.00	0.000	0.000	0.0	0.00	0.000	0.000	0.0	−0.3	0.0	−0.7	0.0	0.2	0.1
32	0.0	−0.001	0.048	30.55	0.144	1.018	161.0	31.15	0.146	1.028	162.6	44.5	28.5	−49.4	21.2	15.3	4.9
32	0.0	0.001	0.045	60.08	0.204	1.419	227.4	61.26	0.206	1.433	229.6	90.0	54.9	−102.6	41.3	27.3	13.6
32	0.0	−1.993	−2.012	60.34	0.204	1.420	227.9	61.59	0.206	1.435	230.3	90.2	14.5	−116.4	42.6	−11.8	−3.5
32	0.0	−0.031	0.013	60.31	0.204	1.419	228.0	61.49	0.206	1.433	230.2	90.1	54.5	−102.9	41.4	26.9	13.2
32	0.0	2.004	2.099	60.21	0.204	1.417	227.8	61.45	0.206	1.432	230.2	94.3	88.3	−92.5	44.5	59.2	27.2
32	0.0	4.027	4.175	60.40	0.204	1.418	228.3	61.74	0.207	1.434	230.8	102.5	124.0	−84.8	50.9	91.5	38.6
32	0.0	5.949	6.138	59.90	0.203	1.412	227.3	61.32	0.206	1.428	230.0	113.1	155.8	−74.5	58.7	116.8	52.7
32	0.0	2.023	2.120	60.21	0.204	1.415	227.9	61.46	0.206	1.430	230.3	94.6	88.9	−93.0	44.8	59.8	26.7
32	0.0	0.035	0.080	60.36	0.204	1.417	228.2	61.54	0.206	1.430	230.5	90.1	55.7	−102.9	41.5	28.1	13.3
32	0.0	0.017	0.017	0.00	0.000	0.000	0.0	0.00	0.000	0.000	0.0	0.4	0.2	−3.5	0.0	0.4	−2.7
32	0.0	0.018	0.018	0.00	0.000	0.000	0.0	0.00	0.000	0.000	0.0	0.4	0.2	−3.4	0.0	0.4	−2.6
33	45.0	0.017	0.017	0.01	0.002	0.017	2.7	0.01	0.002	0.017	2.7	0.0	0.2	−1.9	−0.2	0.4	−1.1
33	45.0	0.021	0.048	30.14	0.143	1.009	160.1	30.69	0.145	1.018	161.5	42.4	22.0	−41.2	19.1	8.8	13.2
33	45.0	0.024	0.046	59.81	0.203	1.413	227.0	60.92	0.205	1.426	229.1	85.5	41.6	−84.3	36.8	14.0	31.9
33	45.0	−2.000	−2.057	60.59	0.205	1.420	228.6	61.90	0.207	1.435	231.1	86.6	−10.3	−109.0	39.0	−36.6	3.9
33	45.0	−0.018	0.003	59.95	0.204	1.412	227.4	61.06	0.205	1.425	229.5	86.0	40.8	−85.9	37.4	13.3	30.2
33	45.0	2.005	2.109	60.01	0.204	1.412	227.6	61.30	0.206	1.427	230.0	88.8	95.5	−61.4	39.0	66.4	58.2
33	45.0	3.979	4.164	60.49	0.205	1.417	228.6	61.92	0.207	1.434	231.2	95.9	151.2	−38.9	44.5	118.8	84.4
33	45.0	5.984	6.251	60.47	0.204	1.417	228.5	62.00	0.207	1.435	231.4	107.6	210.9	−14.7	53.6	171.8	112.6
33	45.0	1.998	2.102	60.53	0.205	1.418	228.6	61.83	0.207	1.433	231.1	88.8	95.3	−60.6	39.1	66.2	59.0
33	45.0	−0.023	−0.002	59.88	0.203	1.410	227.4	60.99	0.205	1.423	229.5	85.6	40.3	−85.1	37.0	12.8	31.0
33	45.0	−0.033	−0.033	0.00	0.001	0.009	1.5	0.00	0.001	0.010	1.5	0.4	0.2	−3.0	0.2	0.4	−2.2